# Motion of the charged test particles in Kerr-Newman-Taub-NUT spacetime and analytical solutions

Hakan Cebeci*
Department of Physics, Anadolu University, 26470 Eskişehir, Turkey

Nülifer Özdemir†
Department of Mathematics, Anadolu University, 26470 Eskişehir, Turkey

Seçil Şentorun‡
Department of Physics, Anadolu University, 26470 Eskişehir, Turkey

**Abstract**

In this work, we study the motion of charged test particles in Kerr-Newman-Taub-NUT spacetime. We analyze the angular and the radial parts of the orbit equations and examine the possible orbit types. We also investigate the spherical orbits and their stabilities. Furthermore, we obtain the analytical solutions of the equations of motion and express them in terms of Jacobian and Weierstrass elliptic functions. Finally, we discuss the observables of the bound motion and calculate the perihelion shift and Lense-Thirring effect for three dimensional bound orbits.

PACS numbers: 04.20Jb, 02.30.Gp, 02.30.Hq

*E.mail: hcebeci@anadolu.edu.tr
†E.mail: nozdemir@anadolu.edu.tr
‡E.mail: secilo@anadolu.edu.tr

# 1 Introduction

The Kerr-Newman-Taub-NUT spacetime is known as a stationary axially symmetric solution of Einstein-Maxwell field equations. The spacetime represents a rotating electrically charged source equipped with a gravitomagnetic monopole moment which is also identified as the NUT charge [1, 2]. The solution contains four physical parameters: The gravitational mass, which is also called gravitoelectric charge; the gravitomagnetic mass (also known as the NUT charge); the rotation parameter that is the angular speed per unit mass and electric charge associated with the Maxwell field. As is well known, the NUT charge produces an asymptotically non-flat spacetime in contrast to Kerr geometry that is asymptotically flat [3]. Although the Kerr-Newman-Taub-NUT spacetime has no curvature singularities, there exist conical singularities on the axis of symmetry as in its uncharged version (namely the Kerr-Taub-NUT spacetime) [4]. One can get rid off conical singularities by taking a periodicity condition over the time coordinate. But, this leads to the emergence of closed time-like curves in the spacetime as in its uncharged version. It means that, in contrast to Kerr and Kerr-Newman solutions interpreted as regular rotating black holes, the Kerr-Newman-Taub-NUT solution cannot be identified as a regular black hole solution due to its singularity structure. Although charged and uncharged spacetimes with NUT parameter have unpleasing physical properties, its worth to investigate such spacetimes in general relativity due to their asymptotically non-flat spacetime structures. To explore their various physical phenomena the spacetimes with NUT charge have been vastly studied in the works [5, 6, 7, 8, 9, 10, 11, 12] where in [5], an alternative physical interpretation of the NUT parameter is also illustrated.

One way to explore the properties of Kerr-Newman-Taub-NUT spacetime is to study the motion of (charged) test particles in this background. One can solve the equations of motion analytically and examine the effect of the NUT parameter and charge of the test particle. Moreover, by integrating equations of motion for bound orbits, one can also calculate the precession of the orbital motion and Lense-Thirring effect.

The geodesic motion of test particles were first examined analytically in Schwarzchild spacetime in [13]. Later on, the motion of test particles was extensively investigated in Kerr spacetimes where the circular geodesics has also been examined [14, 15, 16, 17]. Recently, in [18], analytic solutions of the bound timelike geodesics of test particles in Kerr spacetime

have been presented in terms of elliptic integrals using Mino time. In [19] and [20], the geodesic equations are analytically solved in the background of Schwarzschild-(anti) de Sitter spacetimes, where the solutions are expressed in terms of Kleinian sigma functions. In [21], investigation of analytic solutions has been extended to Kerr-(anti) de Sitter spacetimes where in this case the solutions are presented in terms of Weierstrass elliptic functions. In a similar fashion, geodesic equations are solved in the spacetime of Kerr black hole pierced by a cosmic string [22], where the perihelion shift and Lense-Thirring effect have also been investigated for bound orbits. In [23], the geodesic equations are analytically examined in the background of Einstein-Maxwell-dilaton-axion black hole, where the effect of dilaton charge is investigated. Similarly, analytic solutions of geodesic equations are given in higher dimensional static spherically symmetric spacetimes [24]. Likewise, in [25] and [26], the equation of geodesic motion have been examined in singly and doubly spinning black ring spacetimes respectively. In addition, the orbital motion of electrically and magnetically charged test particles have been studied in the background of Reissner-Nordström [27] and Kerr-Newman spacetimes [28], where the effect of the charge of the test particle has been observed.

In this work, using Hamilton-Jacobi method, we derive the equations of motion for a charged test particle in the background of Kerr-Newman-Taub-NUT spacetime. By making a transformation on the time variable, we decouple the radial and angular ($\theta-$)part of the equations of motion and express all the differential equations in terms of Mino time [29]. We analyze the angular and radial part of the orbit equations and examine the possible orbit types including the special spherical orbits. Furthermore, we obtain the energy and the orbital angular momentum of the test particle for a spherical orbit. We also examine the stability of spherical orbits with respect to NUT parameter. Next, we present the analytical solutions of the equations of the motion by expressing them in terms of Weierstrass $\wp$, $\sigma$, and $\zeta$ functions. Additionally, we calculate the angular frequencies for the bounded radial and angular motions and examine the perihelion precision and the Lense-Thirring effect.

Organization of the paper is as follows: In section 2, we introduce Kerr-Newman-Taub-NUT spacetime. In section 3, we derive the equations of motion of the test particles by expressing them in terms of Mino time as well. In section 4, we make a comprehensive analysis of the angular and radial motion where we also examine the spherical orbits as a subsection. In chapter 5, we give detailed analytical solutions of all the equations that describe the

orbital motion. Next, we discuss possible orbit types by obtaining plots of the different orbits with respect to spacetime parameters, the charge, the energy and the orbital angular momentum of the test particle. We also calculate and examine perihellion precision and the Lense-Thirring effect for the bound orbits. We end up with some comments and conclusions.

# 2 Kerr-Newman-Taub-NUT spacetime

The Kerr-Newman-Taub-NUT spacetime is a stationary solution of the Einstein-Maxwell field equations that is asymptotically non-flat. The metric describes a rotating electrically charged source that also includes a NUT charge which is also known as gravitomagnetic monopole moment. In Boyer-Lindquist coordinates, Kerr-Newman-Taub-NUT spacetime can be described by the metric with asymptotically non-flat structure,

$$g = -\frac{\Delta}{\Sigma}(dt - \chi d\varphi)^2 + \Sigma\left(\frac{dr^2}{\Delta} + d\theta^2\right) + \frac{\sin^2\theta}{\Sigma}\left(adt - (r^2 + \ell^2 + a^2)d\varphi\right)^2 \tag{2.1}$$

where

$$\begin{aligned} \Sigma &= r^2 + (\ell + a\cos\theta)^2, \\ \Delta &= r^2 - 2Mr + a^2 - \ell^2 + Q^2, \\ \chi &= a\sin^2\theta - 2\ell\cos\theta. \end{aligned} \tag{2.2}$$

Here, $M$ is a parameter related to physical mass of the gravitational source. $a$ is associated with its angular momentum per unit mass and $\ell$ denotes gravitomagnetic monopole moment of the source which is also identified as the NUT charge. $Q$ is the electric charge. For future use, we also include the inverse metric components:

$$g^{tt} = -\frac{1}{\Delta\Sigma}\left\{(r^2 + a^2 + \ell^2)^2 - a^2\sin^2\theta\Delta + 4\ell\Delta\frac{\cot\theta}{\sin\theta}(\chi + \ell\cos\theta)\right\}, \tag{2.3}$$

$$g^{rr} = \frac{\Delta}{\Sigma}, \quad g^{\theta\theta} = \frac{1}{\Sigma}, \quad g^{\varphi\varphi} = \frac{1}{\Delta\Sigma\sin^2\theta}(\Delta - a^2\sin^2\theta), \tag{2.4}$$

$$g^{t\varphi} = -\frac{1}{\Delta\Sigma}\left\{(2Mr + 2\ell^2 - Q^2)a + 2\ell\Delta\frac{\cot\theta}{\sin\theta}\right\}. \tag{2.5}$$

The electromagnetic field of the source can be given by the potential 1-form

$$A = -\frac{Qr}{\Sigma}(dt - \chi d\varphi) = A_t dt + A_\varphi d\varphi, \tag{2.6}$$

where

$$A_t = -\frac{Qr}{\Sigma}, \qquad A_\varphi = \frac{\chi Qr}{\Sigma}. \tag{2.7}$$

Interestingly, although the spacetime cannot be identified as a black hole, it has metric singularities at the locations

$$r_\pm = M \pm \sqrt{M^2 - a^2 + \ell^2 - Q^2}, \tag{2.8}$$

where $\Delta = 0$. It can be seen that, the spacetime allows a family of locally non-rotating observers which rotate with coordinate angular velocity given by

$$\Omega = -\frac{g_{t\phi}}{g_{\phi\phi}} = \frac{\Delta\chi - a\sin^2\theta(r^2 + \ell^2 + a^2)}{\Delta\chi^2 - \sin^2\theta(r^2 + \ell^2 + a^2)^2}. \tag{2.9}$$

Then, at the outermost singularity $r_+$, the angular velocity can be calculated as

$$\Omega_+ = -\left(\frac{g_{t\phi}}{g_{\phi\phi}}\right)\Big|_{r=r_+} = \frac{a}{r_+^2 + \ell^2 + a^2}\,. \tag{2.10}$$

It is also obvious that the Killing vectors $\xi_{(t)}$ and $\xi_{(\phi)}$ generate two constants of motion namely the energy and the angular momentum. It can be shown that the Killing vector $\xi = \xi_{(t)} + \Omega_+ \xi_{(\phi)}$ becomes null at the metric singularity where $r = r_+$.

# 3 The motion of charged test particles

In this section, we examine the motion of charged test particle in Kerr-Newman-Taub-NUT spacetime. We choose the units such that we take the speed of light $c = 1$. To this end, we introduce the Hamilton-Jacobi equation for a charged particle

$$2\frac{\partial S}{\partial \tau} = g^{\mu\nu}\left(\frac{\partial S}{\partial x^\mu} - qA_\mu\right)\left(\frac{\partial S}{\partial x^\nu} - qA_\nu\right) \tag{3.1}$$

where $\tau$ is an affine parameter and $q$ is the charge of the particle. Since the spacetime (2.1) admits the timelike Killing vector $\xi_{(t)}$ and spacelike Killing

vector $\xi_{(\phi)}$, the solution of the Hamilton-Jacobi equation can be written as

$$S = -\frac{1}{2}m^2\tau - Et + L\varphi + f(r,\theta) \tag{3.2}$$

where $f(r,\theta)$ is a function of the variables $r$ and $\theta$, the constants of motion $m$, $E$ and $L$ denote the mass, the energy and the angular momentum of the particle respectively. Furthermore, the separability of the Hamilton-Jacobi equation [30, 31, 32] in Kerr-Newman-Tab-NUT spacetime implies that the function $f(r,\theta)$ can be expressed as a sum of two different functions which only depend on $r$ and $\theta$ independently, i.e.

$$f(r,\theta) = S_r(r) + S_\theta(\theta). \tag{3.3}$$

The substitution of (3.3) together with (2.3), (2.4), (2.5), (2.7) and (3.2) into Hamilton-Jacobi equation (3.1) results in two differential equations

$$\left(\frac{dS_r}{dr}\right)^2 = \frac{1}{\Delta}\left\{-K - m^2r^2 + \frac{1}{\Delta}\left[(r^2+a^2+\ell^2)E - aL - qQr\right]^2\right\} \tag{3.4}$$

and

$$\left(\frac{dS_\theta}{d\theta}\right)^2 = K - m^2(\ell + a\cos\theta)^2 - \left(\frac{\chi E - L}{\sin\theta}\right)^2, \tag{3.5}$$

where $K$ can be identified as the Carter separability constant. Using canonical momenta $P_\mu$ expression

$$P_\mu = \frac{\partial S}{\partial x^\mu} = mg_{\mu\nu}\frac{dx^\nu}{d\tau} + qA_\mu \tag{3.6}$$

and identifying

$$P_t = -E, \qquad P_\varphi = L \tag{3.7}$$

we obtain the following equations of motion:

$$\frac{dr}{d\tau} = \mp\frac{1}{\Sigma}\sqrt{\left[(r^2+\ell^2+a^2)\bar{E} - a\bar{L} - \bar{q}Qr\right]^2 - \Delta\left(\frac{K}{m^2} + r^2\right)}, \tag{3.8}$$

$$\frac{d\theta}{d\tau} = \mp\frac{1}{\Sigma}\sqrt{\frac{K}{m^2} - (\ell + a\cos\theta)^2 - \left(\frac{\chi\bar{E} - \bar{L}}{\sin\theta}\right)^2}, \tag{3.9}$$

$$\begin{aligned}\frac{dt}{d\tau} &= \frac{1}{\Sigma\Delta\sin^2\theta}\left[\bar{L}\left(\Delta\chi - a\sin^2\theta(r^2+\ell^2+a^2)\right)\right. \\ &+ \left.\bar{E}\left(-\Delta\chi^2 + \sin^2\theta(r^2+\ell^2+a^2)^2\right) - \bar{q}Qr\sin^2\theta(r^2+\ell^2+a^2)\right], \end{aligned} \tag{3.10}$$

$$\begin{aligned}\frac{d\varphi}{d\tau} &= \frac{1}{\Sigma\Delta\sin^2\theta}\left[\bar{E}\left(-\Delta\chi + asin^2\theta(r^2+\ell^2+a^2)\right)\right. \\ &+ \left.\bar{L}\left(\Delta - a^2 sin^2\theta\right) - \bar{q}Qrasin^2\theta\right] \end{aligned} \tag{3.11}$$

where we define

$$\bar{E} := \frac{E}{m}, \qquad \bar{L} := \frac{L}{m}, \qquad \bar{q} := \frac{q}{m}\cdot \tag{3.12}$$

Defining a new time parameter $\lambda$ (the so-called Mino time) as in [29] such that

$$\frac{d\lambda}{d\tau} = \frac{1}{\Sigma}, \tag{3.13}$$

we can express the equations of motion in terms of the new time parameter:

$$\frac{dr}{d\lambda} = \mp\sqrt{P_r(r)}, \tag{3.14}$$

$$\frac{d\theta}{d\lambda} = \mp\sqrt{P_\theta(\theta)}, \tag{3.15}$$

$$\begin{aligned}\frac{dt}{d\lambda} &= \frac{\chi(\bar{L}-\bar{E}\chi)}{\sin^2\theta\sqrt{P_\theta(\theta)}}\frac{d\theta}{d\lambda} \\ &+ (\bar{E}(r^2+a^2+\ell^2) - a\bar{L} - \bar{q}Qr)\frac{(r^2+a^2+\ell^2)}{\Delta\sqrt{P_r(r)}}\frac{dr}{d\lambda}, \end{aligned} \tag{3.16}$$

$$\begin{aligned}\frac{d\varphi}{d\lambda} &= \frac{(\bar{L}-\bar{E}\chi)}{\sin^2\theta\sqrt{P_\theta(\theta)}}\frac{d\theta}{d\lambda} \\ &+ \frac{a\left[(r^2+a^2+\ell^2) - \bar{L}a - \bar{q}Qr\right]}{\Delta\sqrt{P_r(r)}}\frac{dr}{d\lambda}, \end{aligned} \tag{3.17}$$

where

$$P_r(r) = \left[(r^2+\ell^2+a^2)\bar{E} - a\bar{L} - \bar{q}Qr\right]^2 - \Delta\left(\frac{K}{m^2} + r^2\right) \tag{3.18}$$

and

$$P_\theta(\theta) = \frac{K}{m^2} - (\ell + a\cos\theta)^2 - \left(\frac{\chi\bar{E}-\bar{L}}{\sin\theta}\right)^2. \tag{3.19}$$

# 4 Analysis of the motion:

In this part, we make an analysis or angular and radial motion and examine the possible orbit types. We also investigate the stability of spherical orbits.

## 4.1 Analysis of the angular motion ($\theta$-motion)

Writing the angular equation as

$$\left(\frac{d\theta}{d\lambda}\right)^2 = P_\theta(\theta), \tag{4.1}$$

we see that $P_\theta(\theta) \geq 0$ for the possibility of the motion where $P_\theta(\theta)$ can also be interpreted as the potential associated with the angular motion. Obviously, it depends on the relation between spacetime parameters $a$, $M$, $\ell$ and the energy and the angular momentum of the test particle. Associated with these parameters, either the motion is not possible (i.e $P_\theta(\theta) < 0$ ) or it is confined to an angular interval where $\theta_1 \leq \theta \leq \theta_2$ (i.e the angular motion is bound). We should also comment that depending on the values of the parameters, $\theta = \frac{\pi}{2}$ can be included in that angular interval or not. It means that, the angular motion of the test particle is bound such that the particle can cross or cannot cross the equatorial plane depending on the spacetime parameters. From the expression of $P_\theta(\theta)$, one can easily see that if the condition

$$\frac{K}{m^2} \geq \ell^2 + (\bar{L} - a\bar{E})^2 \tag{4.2}$$

is satisfied, the test particle can cross the equatorial plane ($\theta = \frac{\pi}{2}$). Otherwise, the particle cannot pass through the equatorial plane but its motion is restricted to $\theta_1 < \theta < \theta_2$, $\theta = \frac{\pi}{2}$ being outside of this interval. We further remark that, the physical condition $P_\theta(\theta)$ requires that when the spacetime parameters (NUT parameter, rotation parameter) are fixed, a constraint relation between the energy and the angular momentum of the test particle can be developed as is also illustrated in [22]. Nevertheless, for our case, due to the presence of NUT parameter $\ell$, it is very cumbersome to get such a relation between the energy, angular momentum for non-vanishing spacetime parameters.
In the graphs (1a), (1b) and (1c), the angular potential $P_\theta(\theta)$ is plotted with respect to angular variable $\theta$ where it can be seen that there may exist

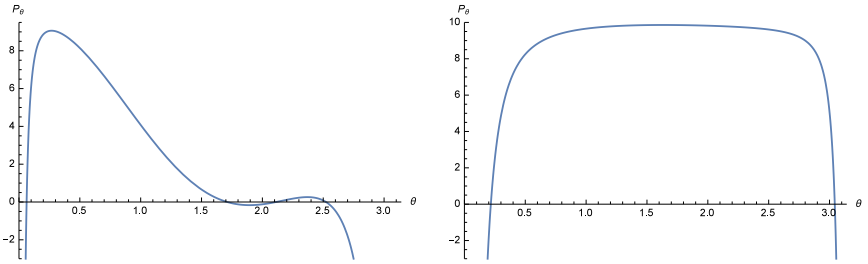


(a) $\bar{L} = -0.4$, $K = 10$, $\bar{E} = 3$ (b) $\bar{L} = 0.5$, $K = 10$, $\bar{E} = 0.96$

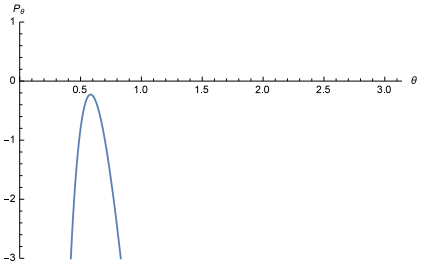


(c) $\bar{L} = 0.5$, $K = 0.5$, $\bar{E} = 5$

Figure 1: Graphs of $P_\theta(\theta)$ with parameters $M = 1$, $a = 0.9$, $\ell = 0.1$, $Q = 0.4$, $\bar{q} = 0.3$ and $m = 1$

one or two angular bound orbits or no motion. It is seen that in the plot (1a), there exist two angular intervals for which $P_\theta(\theta) \geq 0$. In the plot (1b) however, only one physical interval seems to exist for the given spacetime parameters. In both plots, it is also understood that the test particle can cross the equatorial plane (since when $\theta = \frac{\pi}{2}$, $P_\theta(\theta) > 0$). On the other hand, there exists no angular motion in plot (1c) since the condition $P_\theta(\theta) > 0$ is not satisfied for the given spacetime parameters.
In addition, it is also obvious that when

$$P_\theta(\theta) = 0 \tag{4.3}$$

and

$$\frac{dP_\theta(\theta)}{d\theta} = 0, \tag{4.4}$$

the motion is confined to $\theta = \theta_0$ plane. These conditions lead to the following equations:

$$\frac{K}{m^2}\bigg|_{\theta=\theta_0} = (\ell + a\cos\theta_0)^2 + \left(\frac{\chi_0\bar{E} - \bar{L}}{\sin\theta_0}\right)^2 =: \frac{K_0}{m^2}, \tag{4.5}$$

$$a(\ell + a\cos\theta_0)\sin\theta_0 - \frac{\left(\chi_0\bar{E} - \bar{L}\right)}{\sin\theta_0}\left[a\cos\theta_0\bar{E} + \frac{2\ell\bar{E} + \bar{L}\cos\theta_0}{\sin^2\theta_0}\right] = 0, \quad (4.6)$$

where

$$\chi_0 = a\sin^2\theta_0 - 2\ell\cos\theta_0. \quad (4.7)$$

By an analytic calculation, it can be seen that $\theta = \frac{\pi}{2}$ is not the solution of these equations for arbitrary values of the parameters $\ell$, $a$, $\bar{E}$ and $\bar{L}$. This means that for arbitrary values of gravitomagnetic monopole moment $\ell$ ($\ell \neq 0$), there exist no equatorial plane orbits (also called equatorial geodesics for the motion of uncharged test particle) as is also clearly stated in [6]. On the other hand, for $\ell = 0$, $\theta = \frac{\pi}{2}$ solves the above equations provided that the Carter constant becomes

$$\frac{K}{m^2} = (a\bar{E} - \bar{L})^2. \quad (4.8)$$

It can be seen that, in the vanishing of gravitomagnetic monopole moment, equatorial plane orbits can exist for arbitrary values of the parameters $a$, $\bar{E}$ and $\bar{L}$. Interestingly, the equation (4.4) and (4.5) also admit the solution $\theta_0 = \frac{\pi}{2}$, if the constraint relation

$$\bar{L} = \frac{a(2\bar{E}^2 - 1)}{2\bar{E}} \quad (4.9)$$

is imposed between the angular momentum and the energy of the test particle for arbitrary NUT parameter, provided that the Carter constant becomes $\frac{K_0}{m^2} = \ell^2 + \frac{a^2}{4\bar{E}^2}$ in that case. It means that if the relation (4.9) is satisfied, the test particle is confined to equatorial plane. Therefore, equatorial orbits can also exist for arbitrary NUT parameter if the constraint relation (4.9) holds between the angular momentum and the energy of the test particle and also the spacetime rotation parameter. To our knowledge, this is a new result that has not been mentioned in previous works.

One can also examine the case with vanishing rotation parameter $a$ for $\ell \neq 0$. It can be algebraically seen that when $a = 0$, the motion of the charged particle is restricted to a cone with opening angle determined by either $\cos\theta_0 = -\frac{\bar{L}}{2\ell\bar{E}}$ or $\cos\theta_0 = -\frac{2\ell\bar{E}}{\bar{L}}$. It implies that in the vanishing of the rotation parameter, equatorial orbit may also exist either for the interesting case $\bar{L} = 0$ (and $\ell \neq 0$) or for the case $\ell = 0$ (and $\bar{L} \neq 0$) which is also discussed in [6] for the uncharged particle motion. As a further remark, we should also point out that, the presence of the charge $Q$ associated with the

electromagnetic field and the charge $q$ of the test particle does not affect the angular motion.

## 4.2 Analysis of the radial motion ($r$-motion)

First, we express the radial equation (3.8) in the form

$$\left(\frac{dr}{d\lambda}\right)^2 = P_r(r) \tag{4.10}$$

where $P_r(r)$ is a fourth order polynomial in $r$ with real coefficients. As in the angular case, the possibility of the motion requires that $P_r(r) \geq 0$. Then for $r$-motion, according to the roots of the polynomial $P_r(r)$, one can identify the following orbit types:

**i.** Bound Orbit: If the particle moves in a region $r_2 < r < r_1$, then the motion is bound. This can happen if $P_r(r)$ has four positive real roots or two positive real roots (with two complex roots) or two positive double roots or one triple positive root and one real positive root. In such a case, there may exist one or two bound regions.

**ii.** Flyby Orbit: If the particle starts from $\mp\infty$, and comes to a point $r = r_1$ and goes back to infinity, then the orbit is flyby. Likewise, flyby orbits can be seen when $P_r(r)$ has four positive real roots or two positive real roots (with two complex roots) or two positive double roots or one triple positive root and one real positive root. Similarly, for this case, there may exist one or two flyby orbits.

**iii.** Transit Orbit: If the particle starts from $\mp\infty$, crosses $r = 0$ and goes to $\mp\infty$, then the orbit is transit. This is possible if $P_r(r)$ has no real roots.

**iv.** Spherical Orbit: This is a special type of orbit, such that $P_r(r)$ has a real double root at $r = r_s$.

Depending on the value of the energy of the test particle, one can further examine the possible orbit types:

**1.** For $\bar{E} < 1$: In that case, for physically acceptable motion $P_r(r)$ can have two or four real zeros since as $r \to \mp\infty$, $P_r(r) \to -\infty$. Then, there exist

either one bound orbit or two bound orbits.

**2.** For $\bar{E} > 1$: For this case, possible types of orbits can be classified according to whether $P_r(r)$ has four real zeros, two real zeros or no real zeros. When $P_r(r)$ has no real zeros (in other words all the roots are complex), then only the transit orbit is possible since in that case as $r \to \mp\infty$, $P_r(r) \to \infty$. On the other hand, if $P_r(r)$ has two different real zeros (and two complex conjugate roots), one can get two flyby orbits. Moreover, if $P_r(r)$ has four different real zeros, there exist either two bound orbits or one bound two flyby orbits or even two bound two flyby orbits.

**3.** For $\bar{E} = 1$: For this special case, $P_r(r)$ can possess either three real roots or one real root (with two complex conjugate roots). When $P_r(r)$ has three real roots, one can get bound and flyby orbits. In the case that $P_r(r)$ has only one real root, the possible orbit type is flyby.
In the graphs (2a), (2b) and (2c), some possible orbit types are illustrated. For the first graph (2a), $P_r(r)$ has no real roots so that the orbit is transit type. In graphs (2b) and (2c), there exist one and two bound regions respectively.
Alternatively, one can express the equation (4.10) as

$$\left(\frac{dr}{d\lambda}\right)^2 = (r^2 + \ell^2 + a^2)^2 \left(\bar{E} - V_+(r)\right)\left(\bar{E} - V_-(r)\right) \tag{4.11}$$

where

$$V_\pm(r, \bar{L}, a, \ell, \bar{q}, Q) = \frac{a\bar{L} + \bar{q}Qr \pm \sqrt{\Delta(r)\left(\frac{K}{m^2} + r^2\right)}}{r^2 + \ell^2 + a^2} \tag{4.12}$$

can be identified as the effective radial potentials. When $P_r(r) = 0$, the $r$-motion has turning points determined by

$$\bar{E} = V_\pm\left(r, \bar{L}, a, \ell, \bar{q}, Q\right)\big|_{r=r_0} = \frac{a\bar{L} + \bar{q}Qr_0 \pm \sqrt{\Delta(r_0)\left(\frac{K}{m^2} + r_0^2\right)}}{r_0^2 + \ell^2 + a^2} \tag{4.13}$$

where $r_0$'s denote turning points of the motion. Concentrating on $V_+(r, \bar{L}, a, \ell, \bar{q}, Q)$, one can analyze the characteristics of the radial motion by plotting $V_+$ as a function of distance $r$. One can further see that as $r \to \infty$, $V_+ \to 1$. In the figure 3, different energy levels determine the turning points of the radial

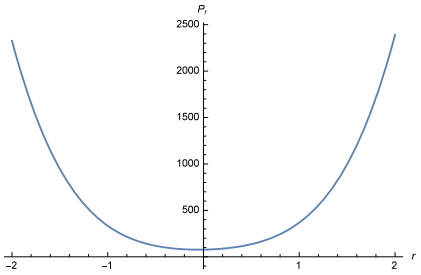


(a) Transit orbit with $\ell = 0.4$, $\bar{E} = 10$

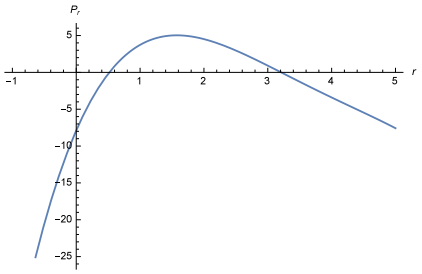


(b) One bound orbit with $\ell = 0.4$, $\bar{E} = 0.94$

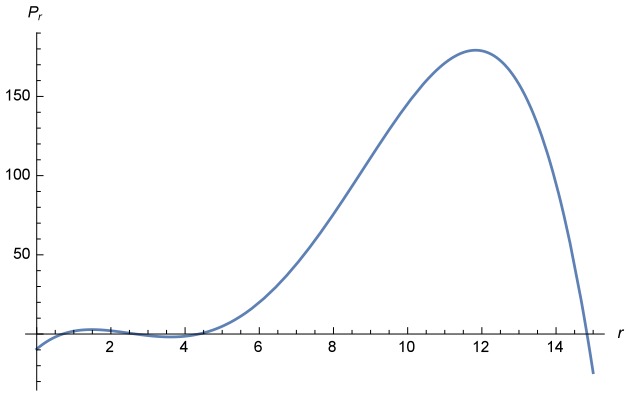


(c) Two bound orbits with $\ell = 0.1$, $\bar{E} = 0.96$

Figure 2: Graphs of $P_r(r)$ with parameters $M = 1$, $a = 0.9$, $K = 10$, $Q = 0.4$, $\bar{q} = 0.3$, $\bar{L} = 0.5$ and $m = 1$.

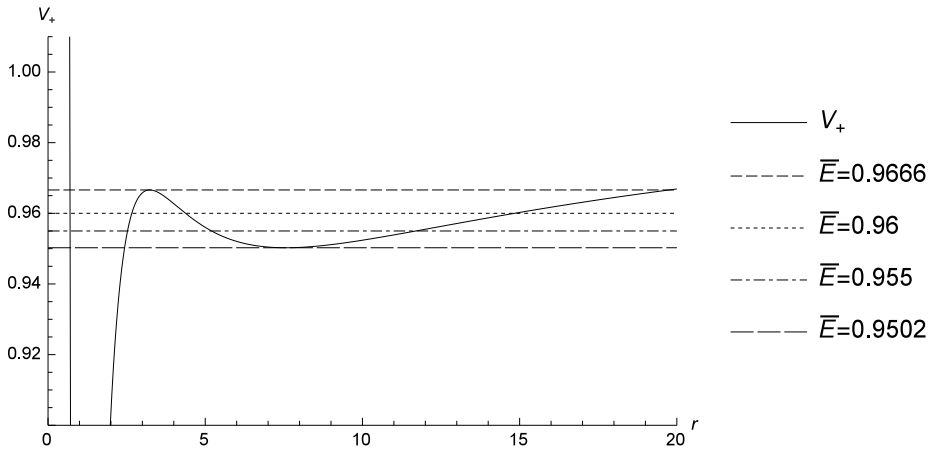


Figure 3: The graph of $V_+$ with parameters $M = 1$, $a = 0.9$, $\ell = 0.1$, $Q = 0.4$, $\bar{q} = 0.3$, $\bar{L} = 0.5$, $K = 10$, $m = 1$ which describes possible types of orbits.

motion. As explicitly illustrated in [14], a bound motion is possible if there exist three or more turning points on the figure of effective potential $V_+$ [14]. It is also illustrative to examine the variation of the effective radial potential for different values of NUT parameter $\ell$ (the other parameters are fixed) and the charge $\bar{q}$ of the test particle. As can be seen from the graphs, the potentials have some local maxima and minima recalling that $P_r(r) \to 1$ as $r \to \infty$. From the first graph, for the fixed parameters $M = 1$, $a = 0.9$, $Q = 0.4$, $\bar{q} = 0.3$, $\bar{L} = 0.5$, $K = 10$ and $m = 1$, one can realize that as the value of NUT parameter $\ell$ increases, local maxima tends to disappear. On the other hand, one can see from the second graph that for the same parameter values (except that we take $\ell = 0.1$ for this case) as the charge $\bar{q}$ of the test particle decreases, the local maxima has a similar behaviour.
It is also of great interest to investigate the existence of the bound orbits in the region where $r > r_+$ (in other words outside the singularity of the spacetime). This means that a radial bound interval $r_1 \leq r \leq r_2$ exists such that for that region, $P_r(r) > 0$ and $r_+ < r_1$. To make an analysis of bound motion similar to [14], we can affect a transformation $r =: R + r_+$, where $r_+$ describes the metric singularity (i.e. $\Delta(r_+) = 0$), assuming that at least one region of binding exists where $r > r_+$. To this end, we express $P_r(r)$ in terms of new variable $R$. Then in terms of $R$, we obtain

$$P_R(R) = A_4 R^4 + A_3 R^3 + A_2 R^2 + A_1 R + A_0 \tag{4.14}$$

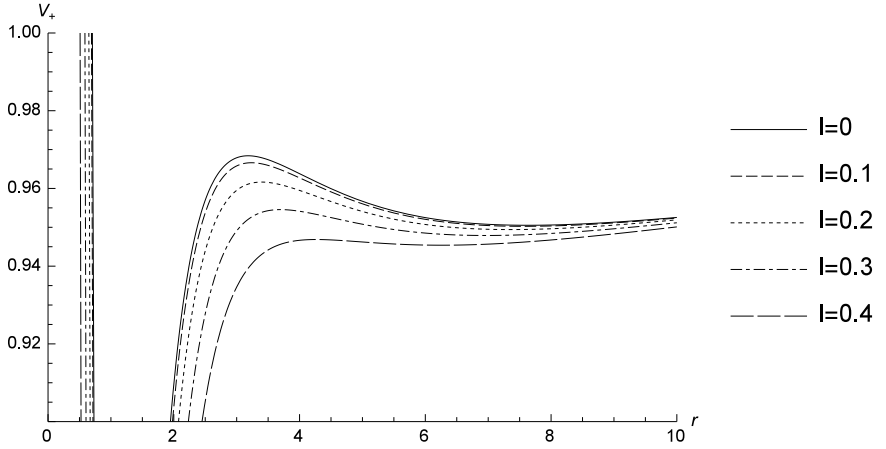


Figure 4: The graph of $V_+$ as a function of $r$, with parameters $M = 1$, $a = 0.9$, $Q = 0.4$, $\bar{q} = 0.3$, $\bar{L} = 0.5$, $K = 10$, $m = 1$ for different values of $\ell$.

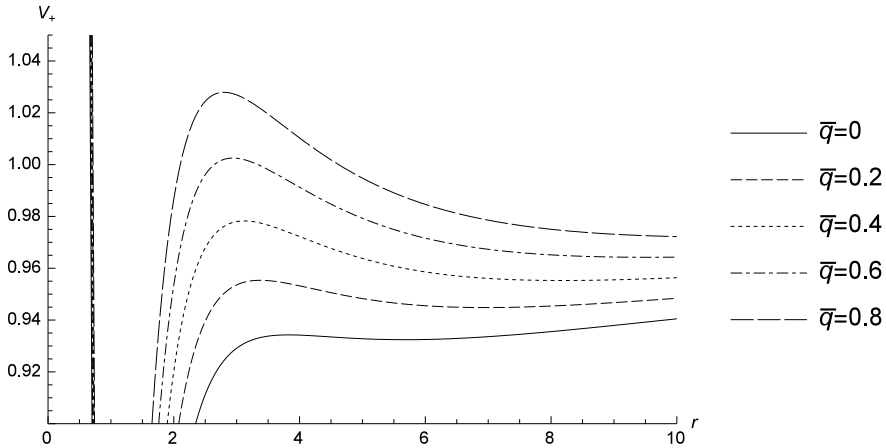


Figure 5: The graph of $V_+$ as a function of $r$, with parameters $M = 1$, $a = 0.9$, $\ell = 0.1$, $Q = 0.4$, $\bar{L} = 0.5$, $K = 10$, $m = 1$ for different values of $\bar{q}$.

where

$$A_0 = \left(\bar{E}(\ell^2 + a^2 + r_+^2) - (a\bar{L} + \bar{q}Qr_+)\right)^2, \tag{4.15}$$

$$\begin{aligned} A_1 &= 4\bar{E}^2 r_+(r_+^2 + \ell^2 + a^2) - 2\bar{E}\left(3\bar{q}Qr_+^2 + 2\bar{L}ar_+ + \bar{q}Q(\ell^2 + a^2)\right) \\ &\quad +2\bar{q}Q(\bar{q}Qr_+ + a\bar{L}) - 2\left(\frac{K}{m^2} + r_+^2\right)(r_+ - M) \end{aligned} \tag{4.16}$$

$$\begin{aligned} A_2 &= 6(\bar{E}^2 - 1)r_+^2 + 6(M - \bar{q}Q\bar{E})r_+ + 2\bar{E}^2(\ell^2 + a^2) \\ &\quad -2\bar{E}\bar{L}a + \bar{q}^2Q^2 - \frac{K}{m^2} - (a^2 - \ell^2 + Q^2) \end{aligned} \tag{4.17}$$

$$A_3 = 2\left(2r_+(\bar{E}^2 - 1) + M - \bar{q}Q\bar{E}\right), \tag{4.18}$$

$$A_4 = \bar{E}^2 - 1. \tag{4.19}$$

At this stage, let us consider in what conditions this polynomial has positive roots. We remark that $A_0 > 0$. According to Descartes' rule of sign, a polynomial possessing real coefficients can not have more positive roots than the number of variations of sign in its coefficients. Then if $A_4 > 0$ ($\bar{E}^2 > 1$), a bound region for $r > r_+$ can be realized under the conditions

$$A_1 < 0, \qquad A_2 > 0, \qquad A_3 < 0 \tag{4.20}$$

since we also have $A_0 > 0$. Then four variations of sign would be possible and therefore there may exist four real positive roots for $P_R(R)$. If the above conditions are simultaneously satisfied, we have the possibility of having at most four turning points and therefore a bound motion may exist for $\bar{E}^2 > 1$. On the other hand, if $A_4 < 0$ ($\bar{E}^2 < 1$), there exist at most three variations of sign since $A_0 > 0$. For this case, then either of the following inequalities should be simultaneously fulfilled for the existence of bound region(s):

$$\begin{array}{lll} A_1 < 0, & A_2 < 0, & A_3 > 0, \\ A_1 > 0, & A_2 < 0, & A_3 > 0, \\ A_1 < 0, & A_2 > 0, & A_3 > 0, \\ A_1 < 0, & A_2 > 0, & A_3 < 0. \end{array} \tag{4.21}$$

Similarly, this implies that if any one of the above conditions are simultaneously satisfied, there exists at most one region of binding outside the outer singularity where $r > r_+$.

## 4.3 The spherical orbits and stability

The spherical orbits are special orbits that satisfy

$$P_r(r = r_s) = 0, \tag{4.22}$$

$$\left.\frac{dP_r}{dr}\right|_{r=r_s} = 0 \tag{4.23}$$

at $r = r_s$. These require that

$$\begin{aligned}
&(\bar{E_s}^2 - 1)r_s^4 + 2(M - \bar{q}Q\bar{E}_s)r_s^3 \\
&+\left(2(\ell^2 + a^2)\bar{E_s}^2 + \bar{q}^2Q^2 - 2a\bar{E}_s\bar{L_s} - \frac{K}{m^2} - (a^2 - \ell^2 + Q^2)\right) r_s^2 \\
&+2\left(\frac{KM}{m^2} + a\bar{q}Q\bar{L_s} - \bar{q}Q(\ell^2 + a^2)\bar{E}_s\right) r_s \\
&+(\ell^2 + a^2)^2\bar{E_s}^2 + a^2\bar{L_s}^2 - 2a(\ell^2 + a^2)\bar{E}_s\bar{L_s} - \frac{K}{m^2}(a^2 - \ell^2 + Q^2) = 0
\end{aligned} \tag{4.24}$$

and

$$\begin{aligned}
&4(\bar{E_s}^2 - 1)r_s^3 + 6(M - \bar{q}Q\bar{E}_s)r_s^2 \\
&+2\left(2(\ell^2 + a^2)\bar{E_s}^2 + \bar{q}^2Q^2 - 2a\bar{E}_s\bar{L_s} - \frac{K}{m^2} - (a^2 - \ell^2 + Q^2)\right) r_s \\
&+2\left(\frac{KM}{m^2} + a\bar{q}Q\bar{L_s} - \bar{q}Q(\ell^2 + a^2)\bar{E}_s\right) = 0.
\end{aligned} \tag{4.25}$$

Considering that $P_r(r)$ can also be written in the form

$$P_r(r) = (r - r_s)^2\left((\bar{E_s}^2 - 1)r^2 + \mu_1 r + \mu_2\right), \tag{4.26}$$

the relations (4.24) and (4.25) can equivalently be expressed in the following forms:

$$\begin{aligned}
&\left[3r_s^4 + 2r_s^2(\ell^2 + a^2) - (\ell^2 + a^2)^2\right]\bar{E_s}^2 - a^2\bar{L_s}^2 + 2a\left(\ell^2 + a^2 - r_s^2\right)\bar{E}_s\bar{L_s} \\
&-4r_s^3\bar{q}Q\bar{E}_s + \left(a^2 - \ell^2 + Q^2\right)\left(\frac{K}{m^2} - r_s^2\right) - r_s^2\left(3r_s^2 - 4r_sM - \bar{q}^2Q^2 + \frac{K}{m^2}\right) = 0
\end{aligned} \tag{4.27}$$

and

$$\begin{aligned}
&2r_s(\ell^2 + a^2 + r_s^2)\bar{E_s}^2 + a\left(\bar{q}Q - 2r_s\bar{E}_s\right)\bar{L_s} - \left(3r_s^2 + \ell^2 + a^2\right)\bar{q}Q\bar{E}_s \\
&+3r_s^2M - \left(\frac{K}{m^2} + a^2 - \ell^2 + Q^2 - \bar{q}^2Q^2 + 2r_s^2\right) r_s + \frac{KM}{m^2} = 0.
\end{aligned} \tag{4.28}$$

Now, we find analytical solutions to the energy and angular momentum of the particle in spherical orbit with radius $r = r_s$. We consider the following cases:

**i.** The case $a \neq 0$ and $\bar{L}_s \neq 0$:

The equations (4.27) and (4.28) lead to a second order equation in $\bar{E}_s$ in the form

$$\nu_2 {\bar{E}_s}^2 + \nu_1 \bar{E}_s + \nu_0 = 0, \tag{4.29}$$

where the coefficients read

$$\begin{aligned} \nu_0 = &- \left[ r_s \left( \bar{q}^2 Q^2 - \Delta(r_s) \right) + (M - r_s) \left( \frac{K}{m^2} + r_s^2 \right) \right]^2 \\ &+ \bar{q}^2 Q^2 \left[ \Delta(r_s) \left( \frac{K}{m^2} - r_s^2 \right) + 2 r_s (M - r_s) \left( \frac{K}{m^2} + r_s^2 \right) + r_s^2 \bar{q}^2 Q^2 \right], \end{aligned} \tag{4.30}$$

$$\nu_1 = -4 \bar{q} Q r_s \left( \frac{K}{m^2} + r_s^2 \right) \Delta(r_s) \tag{4.31}$$

and

$$\nu_2 = 4 r_s^2 \left( \frac{K}{m^2} + r_s^2 \right) \Delta(r_s). \tag{4.32}$$

The equation (4.29) can be solved as

$${\bar{E}_s}^{\pm} = \frac{\bar{q} Q}{2 r_s} \pm \frac{\sqrt{D_s}}{8 r_s^2 \Delta(r_s) \left( \frac{K}{m^2} + r_s^2 \right)} \tag{4.33}$$

where

$$D_s = 16 r_s^2 \Delta(r_s) \left( \frac{K}{m^2} + r_s^2 \right) \left[ (r_s - M) \left( \frac{K}{m^2} + r_s^2 \right) + r_s \Delta(r_s) \right]^2. \tag{4.34}$$

Furthermore, the substitution of $\bar{E}_s$ in (4.28) leads to

$$\begin{aligned} {\bar{L}_s}^{\pm} \;=\; & \frac{\bar{q} Q}{2 a r_s} (a^2 + \ell^2 - r_s^2) \pm \frac{(a^2 + \ell^2 + r_s^2) \sqrt{D_s}}{8 \left( \frac{K}{m^2} + r_s^2 \right) \Delta(r_s) a r_s^2} \\ & \mp \frac{4 r_s}{a \sqrt{D_s}} \left( \frac{K}{m^2} + r_s^2 \right) \left[ (r_s - M) \left( \frac{K}{m^2} + r_s^2 \right) + r_s \Delta(r_s) \right] \Delta(r_s). \end{aligned} \tag{4.35}$$

To get a deeper insight of the analytical expressions of energy and angular momentum, we plot them as a function of gravitomagnetic monopole moment

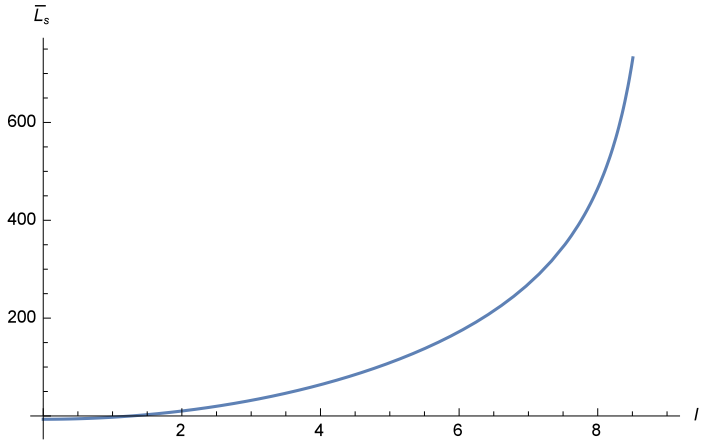


Figure 6: The graph of angular momentum $\bar{L}_s$ as a function of gravitomagnetic monopole moment $\ell$ with parameters $M = 1$, $a = 0.4$, $Q = 0.4$, $\bar{q} = 0.3$, $K = 20$, $m = 1$, $r_s = 10$.

$\ell$ and the spherical radius $r_s$. In both plots, we concentrate on $\bar{L}_s^+$ and $\bar{E}_s^+$. First, looking at the graph of $\bar{L}_s^+$ vs $\ell$ for the parameter values given in Figure 6, it can be seen that as gravitomagnetic monopole moment increases, angular momentum also increases becoming zero at some specific value of the NUT parameter i.e at $\ell = \ell_s$. It is also interesting to see that $\bar{L}_s \leq 0$ when $0 \leq \ell \leq \ell_s$, while $\bar{L}_s > 0$ when $\ell > \ell_s$. This can be physically interpreted as such that one obtains retrograde ($\bar{L}_s \leq 0$) spherical orbits for $0 \leq \ell \leq \ell_s$, while for $\ell > \ell_s$, the orbits are seen to be direct spherical orbits. In addition, we should point out that the analytical expression of $\bar{L}_s$ restrict the value of the NUT parameter $\ell$ since in the expression (4.35), $D_s > 0$ should also be imposed.

For the second plot $\bar{L}_s^+$ vs $r_s$, it can be seen that $\bar{L}_s$ decreases to a certain extremal value and then it again increases. It can also be understood that $\bar{L}_s = 0$ at some particular values of spherical radius $r_s$ i.e when $r_s = r_{s_1}$ and $r_s = r_{s_2}$ assuming that $r_{s_2} < r_{s_1}$. The graph similarly illustrates that, one has direct spherical orbits for the radial intervals where $r_s < r_{s_2}$ and $r_s > r_{s_1}$ while one obtains retrograde orbits for the interval $r_{s_2} < r_s < r_{s_1}$.

For the plot of $\bar{E}_s^+$ vs $\ell$, one can see that the energy of the test particle increases while $\ell$ also increases. It is also interesting to understand that, the increase of energy starts from a value where $\bar{E} < 1$ and then it continues to increase to values where $\bar{E} > 1$, the energy becoming unity at some specific

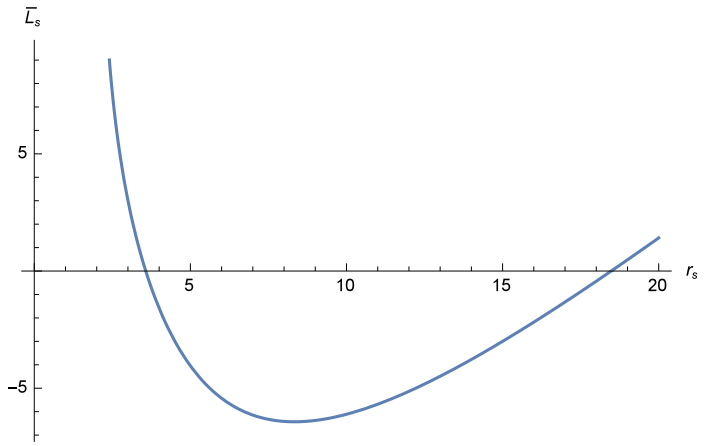


Figure 7: The graph of angular momentum $\bar{L}_s$ as a function of spherical radius $r_s$ with parameters $M = 1$, $a = 0.4$, $\ell = 0.4$, $Q = 0.4$, $\bar{q} = 0.3$, $K = 20$, $m = 1$.

value of NUT parameter $\ell$. It should be also added that value of $\ell$ should again be restricted since the analytic expression (4.33) of $\bar{E}_s$ also suggests that $D_s \geq 0$.
Finally the plot of $\bar{E}_s$ vs $r_s$ shows that, as the value of $r_s$ increases, the energy of test particle starts to decrease from a certain value having an extremum at some specific value of the spherical radius and then it continuous to increase approaching unity (i.e $\bar{E}_s \to 1$) as $r_s \to \infty$.

**ii.** The case $\bar{L}_s = 0$:
For this special case, one can eliminate the Carter constant $\frac{K}{m^2}$ from equation (4.28) and substitute it into the equation (4.27) to obtain the energy equation in the form

$$\bar{\nu_2}\bar{E_s}^{\,2} + \bar{\nu_1}\bar{E}_s + \bar{\nu_0} = 0, \tag{4.36}$$

where in that case the coefficients become

$$\bar{\nu_0} = r_s\left(\Delta^2(r_s) + \bar{q}^2Q^2(-a^2 + \ell^2 - Q^2 + Mr_s)\right), \tag{4.37}$$

$$\bar{\nu_1} = \bar{q}Q\left[a^2(Q^2 + a^2) + \ell^2(Q^2 - \ell^2) + r_s^2(3Q^2 - 2a^2 - 4\ell^2 - 4Mr_s + r_s^2)\right] \tag{4.38}$$

and

$$\bar{\nu_2} = -(a^2 + \ell^2 + r_s^2)\left[\ell^2(M - 3r_s) + a^2(M + r_s) + r_s(2Q^2 - 3Mr_s + r_s^2)\right]. \tag{4.39}$$

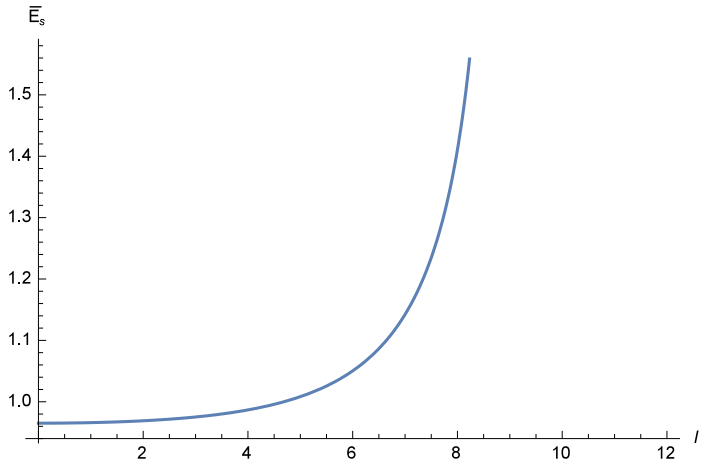


Figure 8: The graph of energy $\bar{E}_s$ as a function of gravitomagnetic monopole moment $\ell$ with parameters $M = 1$, $a = 0.4$, $Q = 0.4$, $\bar{q} = 0.3$, $K = 20$, $m = 1$, $r_s = 10$.

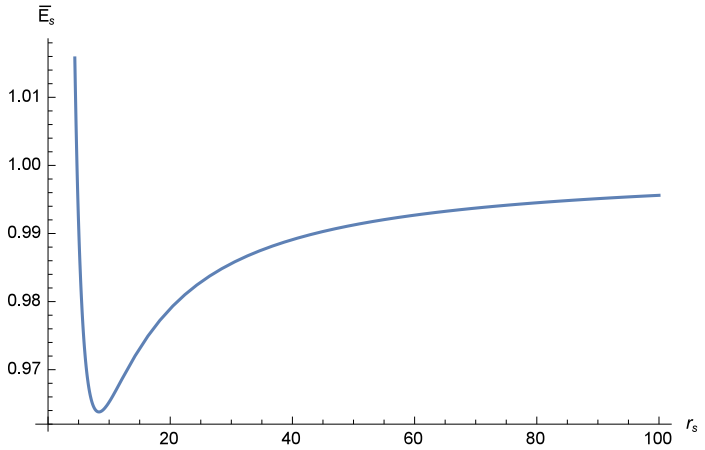


Figure 9: The graph of energy $\bar{E}_s$ as a function of spherical radius $r_s$ with parameters $M = 1$, $a = 0.4$, $\ell = 0.4$, $Q = 0.4$, $\bar{q} = 0.3$, $K = 20$, $m = 1$.

Then the energy can be evaluated as

$$\bar{E_s}^{\pm} = \frac{-\bar{\nu_1} \pm \sqrt{\bar{D_s}}}{2\bar{\nu_2}}, \tag{4.40}$$

where

$$\begin{aligned} \bar{D_s} &= \Delta^2(r_s)\left[4r_s^4(2\Delta(r_s)+r_s(M-r_s))\right. \\ &+\bar{q}^2Q^2r_s^4+(a^2+\ell^2)^2(\bar{q}^2Q^2+4Mr_s) \\ &\left.+2(a^2+\ell^2)r_s^2\left(2\Delta(r_s)-2r_s^2-4\ell^2+2Q^2-\bar{q}^2Q^2\right)\right]. \end{aligned} \tag{4.41}$$

**iii.** The case $a = 0$:
Remarkably, in the case of vanishing angular momentum $a$ (i.e. $a = 0$), but $\bar{q} \neq 0$ which corresponds to spherical orbital motion in Taub-NUT Reissner-Nordström spacetime, again by eliminating the Carter constant from (4.28), one can obtain the following energy equation

$$\tilde{\nu_2}{\bar{E_s}}^2 + \tilde{\nu_1}\bar{E_s} + \tilde{\nu_0} = 0 \tag{4.42}$$

where

$$\tilde{\nu_0} = r_s\left[\bar{q}^2Q^2(\ell^2-Q^2+Mr_s)+(\ell^2-Q^2-r_s(r_s-2M))^2\right], \tag{4.43}$$

$$\tilde{\nu_1} = \bar{q}Q\left[-\ell^4+\ell^2(Q^2-4r_s^2)+r_s^2(3Q^2+r_S(-4M+r_s))\right], \tag{4.44}$$

$$\tilde{\nu_2} = -(\ell^2+r_s^2)\left[\ell^2(M-3r_s)+r_s(2Q^2+r_s(-3M+r_s))\right] \tag{4.45}$$

for arbitrary $\bar{L}$. The solution can be given by

$$\bar{E_s}^{\pm} = \frac{-\tilde{\nu_1} \pm \sqrt{\tilde{D_s}}}{2\tilde{\nu_2}}, \tag{4.46}$$

where

$$\begin{aligned} \tilde{D_s} &= \bar{q}^2Q^2(\ell^2-r_s^2)^2+4r_s\left[\ell^4(M-3r_s)\right. \\ &\left.+r_s^3(2Q^2+r_s^2-3Mr_s)-2\ell^2r_s(r_s^2+r_sM-Q^2)\right]. \end{aligned} \tag{4.47}$$

Now we examine the stability of spherical orbits for arbitrary spacetime parameters. The stability of such orbits implies that [14, 33]

$$\left.\frac{d^2P_r(r)}{dr^2}\right|_{r=r_s} < 0. \tag{4.48}$$

This further leads to the inequality

$$2\left(3r_s^2+\ell^2+a^2\right)\bar{E}^2+2\left(\bar{q}Q-a\bar{L}\right)\bar{E} \tag{4.49}$$
$$-(5r_s+4M)r_s-\Delta(r_s)-\frac{K}{m^2}+\bar{q}^2Q^2<0.$$

This means that the spherical orbits are stable if the energy of the particle falls into the interval

$$\bar{E}_-<\bar{E}<\bar{E}_+, \tag{4.50}$$

where

$$\bar{E}_\pm=\frac{(a\bar{L}-\bar{q}Q)\pm\sqrt{D_E}}{2(3r_s^2+\ell^2+a^2)} \tag{4.51}$$

and

$$D_E=(a\bar{L}-\bar{q}Q)^2+2(3r_s^2+\ell^2+a^2)\left(5r_s^2+4Mr_s+\Delta(r_s)+\frac{K}{m^2}-\bar{q}^2Q^2\right). \tag{4.52}$$

Otherwise, we have an unstable spherical orbit. In Tables 1 and 2, we investigate the stability with respect to change of the NUT parameter $\ell$ and the spherical radius $r_s$. For the values of the spacetime parameters given in tables, as $\ell$ and $r_s$ increases, we obtain that the orbits are all stable. At this stage, we are unable to see an unstable spherical orbit although it is clear that there may exit unstable one(s) for the spacetime parameters that satisfy the inequality (4.49). However looking at the Table 1, stable spherical orbits change their class from retrograde orbits ($a>0,\bar{L}<0$) to direct ones ($a>0,\bar{L}>0$), as the NUT parameter increases. One can see a similar effect in Table 2, when the radius of the spherical orbit is increased.

Table 1: $a=0.4M$, $Q=0.4M$, $r_s=10M$, $M=1$, $\bar{q}=0.3$, $m=1$, $K=20$.

| $\ell$ | $\bar{E}_s^+$ | $\bar{L}_s^+$ | stability of the orbit |
|---|---|---|---|
| 0.1 | 0.965109 | -6.73569 | stable |
| 0.2 | 0.965135 | -6.61086 | stable |
| 0.4 | 0.965241 | -6.1113 | stable |
| 0.8 | 0.965672 | -4.1093 | stable |
| 1.2 | 0.966415 | -0.758978 | stable |
| 2 | 0.969014 | 10.0825 | stable |
| 4 | 0.986713 | 63.9055 | stable |

Table 2: $a = 0.4M$, $Q = 0.4M$, $\ell = 0.4M$, $M = 1$, $\bar{q} = 0.3$, $m = 1$, $K = 20$.

| $r_s$ | $\bar{E}_s^+$ | $\bar{L}_s^+$ | stability of the orbit |
|---|---|---|---|
| 5 | 0.991365 | -4.04398 | stable |
| 10 | 0.965241 | -6.1113 | stable |
| 12 | 0.96844 | -5.13413 | stable |
| 13 | 0.970084 | -4.49053 | stable |
| 15 | 0.973125 | -3.0001 | stable |
| 20 | 0.978958 | 1.41363 | stable |

# 5 Analytical solutions

In this section we investigate and present analytical solutions to $r$-motion, $\theta$-motion, $t$-motion and $\varphi$-motion. We see that the solutions can be expressed in terms of Jacobian elliptic functions $F(y,k)$ and Weierstrass $\wp$, Weierstrass $\sigma$ and Weierstrass $\zeta$ functions.

## 5.1 $\theta$-motion

Making a transformation $x = \cos\theta$, (3.15) can be cast into the following form:

$$\left(\frac{dx}{d\lambda}\right)^2 = C_0 + C_1 x + C_2 x^2 + C_3 x^3 + C_4 x^4 =: P_\theta(x) \tag{5.1}$$

where

$$C_0 = \frac{K}{m^2} - \ell^2 - \left(\bar{L} - a\bar{E}\right)^2 =: \widetilde{K}, \tag{5.2}$$

$$C_1 = 2\ell a(2\bar{E}^2 - 1) - 4\ell\bar{E}\bar{L}, \tag{5.3}$$

$$\begin{aligned} C_2 &= -\frac{K}{m^2} + \ell^2\left(1 - 4\bar{E}^2\right) + a^2\left(\bar{E}^2 - 1\right) + \left(\bar{L} - a\bar{E}\right)^2 - \bar{L}^2 \\ &= -\widetilde{K} - 4\ell^2\bar{E}^2 + a^2\left(\bar{E}^2 - 1\right) - \bar{L}^2, \end{aligned} \tag{5.4}$$

$$C_3 = 2\ell a(1 - 2\bar{E}^2), \tag{5.5}$$

$$C_4 = a^2(1 - \bar{E}^2). \tag{5.6}$$

We also recall that $-1 \leq x \leq 1$. In general, the solution of the fourth order polynomial equation (5.1) can be expressed in terms of elliptic functions. First, we see that the transformation (for $\bar{E} \neq 1$)

$$x = \frac{1}{\xi} + x_\theta \tag{5.7}$$

brings the polynomial equation (5.1) into the following third order form in $\xi$:

$$\left(\frac{d\xi}{d\lambda}\right)^2 = \alpha_3\xi^3 + \alpha_2\xi^2 + \alpha_1\xi + C_4. \tag{5.8}$$

Here $x_\theta$ is a real root of $P_\theta(x)$ and the coefficients are given by

$$\alpha_1 = C_3 + 4C_4x_\theta, \tag{5.9}$$

$$\alpha_2 = C_2 + 3C_3x_\theta + 6C_4x_\theta^2, \tag{5.10}$$

$$\alpha_3 = C_1 + 2C_2x_\theta + 3C_3x_\theta^2 + 4C_4x_\theta^3. \tag{5.11}$$

With the further transformation

$$\xi = \frac{1}{\alpha_3}\left(4y - \frac{\alpha_2}{3}\right), \tag{5.12}$$

we obtain standard Weierstrass form of the differential equation (5.8)

$$\left(\frac{dy}{d\lambda}\right)^2 = 4y^3 - g_2y - g_3 \tag{5.13}$$

where

$$g_2 = \frac{1}{4}\left(\frac{\alpha_2^2}{3} - \alpha_1\alpha_3\right) \tag{5.14}$$

and

$$g_3 = \frac{1}{8}\left(\frac{\alpha_1\alpha_2\alpha_3}{6} - \frac{C_4\alpha_3^2}{2} - \frac{\alpha_2^3}{27}\right). \tag{5.15}$$

The solution of equation (5.13) can be given by Weierstrass $\wp$ function

$$y(\lambda) = \wp\left(\lambda - \lambda_0; g_2, g_3\right), \tag{5.16}$$

where $\lambda_0$ describes the initial Mino time. Hence the solution of $\theta-$equation can be obtained as

$$\theta(\lambda) = \arccos\left(\frac{\alpha_3}{4\wp(\lambda - \lambda_0; g_2, g_3) - \frac{\alpha_2}{3}} + x_\theta\right), \tag{5.17}$$

where the solution is valid for all types of orbits. For that solution, one can assume that there exist at least one real root (in fact there can exist at least two real roots for a fourth order polynomial).
Alternatively, there may exist orbits for which the polynomial $P_\theta(x)$ has four real roots. For the orbits $\bar{E}^2 < 1$ ($C_4 > 0$), one can assume $P_\theta(x)$ has real roots $x_1$, $x_2$, $x_3$, $x_4$ ordered as $x_4 < x_3 < x_2 < x_1$. In this case, there exist three intervals namely $x \leq x_4$, $x_3 \leq x \leq x_2$ and $x \geq x_1$ where $P_\theta(x) \geq 0$ [34]. For the intervals $x \leq x_4$ or $x \geq x_1$, one can consider the transformation [1]

$$\frac{x - x_1}{x - x_2} = \frac{x_1 - x_4}{x_2 - x_4} y_\theta^2. \tag{5.18}$$

Then with this transformation,

$$\begin{aligned}
&\int_{x_1}^{x} \frac{dx}{\sqrt{C_0 + C_1 x + C_2 x^2 + C_3 x^3 + C_4 x^4}} \\
&= \frac{2}{\sqrt{C_4 (x_1 - x_3)(x_2 - x_4)}} \int_0^{y_\theta} \frac{dy_\theta}{\sqrt{(1 - k_\theta^2 y_\theta^2)(1 - y_\theta^2)}} \\
&= \frac{2}{\sqrt{C_4 (x_1 - x_3)(x_2 - x_4)}} F(y_\theta, k_\theta),
\end{aligned} \tag{5.19}$$

where $F(y_\theta, k_\theta)$ describes incomplete Jacobian elliptic function of the first kind. Furthermore, we also have

$$\int_{x_1}^{x} \frac{dx}{\sqrt{C_0 + C_1 x + C_2 x^2 + C_3 x^3 + C_4 x^4}} = \int d\lambda = \lambda - \lambda_0. \tag{5.20}$$

So we obtain

$$F(y_\theta, k_\theta) = \sqrt{C_4 (x_1 - x_3)(x_2 - x_4)}\, \frac{(\lambda - \lambda_0)}{2} \tag{5.21}$$

with

$$k_\theta^2 = \frac{(x_1 - x_4)(x_2 - x_3)}{(x_1 - x_3)(x_2 - x_4)}. \tag{5.22}$$

[1] Equivalently, one can apply a similar transformation on the variables such that $\frac{x - x_3}{x - x_4} = \frac{x_2 - x_3}{x_2 - x_4} y_\theta^2$ and obtain the same analytical result for the solution of the angular equation where in that case the transformation is valid when $x_3 \leq x \leq x_2$.

For the orbits where $\bar{E}^2 > 1$ ($C_4 < 0$), as for the case $\bar{E}^2 < 1$, we can still assume four real roots for the polynomial $P_\theta(x)$ ordered as $\bar{x}_4 < \bar{x}_3 < \bar{x}_2 < \bar{x}_1$. In this case, there exist two intervals $\bar{x}_2 \leq \bar{x} \leq \bar{x}_1$ and $\bar{x}_4 \leq \bar{x} \leq \bar{x}_3$ for which $P_\theta(x) \geq 0$. Concentrating on the interval $\bar{x}_2 \leq \bar{x} \leq \bar{x}_1$, one may consider the transformation [2]

$$\frac{\bar{x} - \bar{x}_2}{\bar{x} - \bar{x}_3} = \frac{\bar{x}_1 - \bar{x}_2}{\bar{x}_1 - \bar{x}_3} y_\theta^2. \tag{5.23}$$

leading to the solution

$$F(y_\theta, \tilde{k}_\theta) = \sqrt{-C_4(\bar{x}_1 - \bar{x}_3)(\bar{x}_2 - \bar{x}_4)}\, \frac{(\lambda - \lambda_0)}{2}, \tag{5.24}$$

with

$$\tilde{k}_\theta^2 = \frac{(\bar{x}_1 - \bar{x}_2)(\bar{x}_3 - \bar{x}_4)}{(\bar{x}_1 - \bar{x}_3)(\bar{x}_2 - \bar{x}_4)}. \tag{5.25}$$

For $\bar{E} = 1$, $P_\theta(x)$ becomes a third order polynomial such that the transformation

$$x = \frac{1}{\bar{C}_3}\left(4y - \frac{\bar{C}_2}{3}\right) \tag{5.26}$$

obviously puts the equation (5.1) into standard Weierstrass form

$$\left(\frac{dy}{d\lambda}\right)^2 = 4y^3 - \bar{g}_2 y - \bar{g}_3 \tag{5.27}$$

where in that case

$$\bar{g}_2 = \frac{1}{4}\left(\frac{\bar{C}_2^2}{3} - \bar{C}_1\bar{C}_3\right), \tag{5.28}$$

$$\bar{g}_3 = \frac{1}{8}\left(\frac{\bar{C}_1\bar{C}_2\bar{C}_3}{6} - \frac{\bar{C}_0\bar{C}_3^2}{2} - \frac{\bar{C}_2^3}{27}\right) \tag{5.29}$$

whose solution can similarly be expressed in terms of Weierstrass $\wp$ function as

$$y(\lambda) = \wp(\lambda - \lambda_0; \bar{g}_2, \bar{g}_3) \tag{5.30}$$

leading to $\theta$-solution

$$\theta(\lambda) = \arccos\left(\frac{1}{\bar{C}_3}(4\wp(\lambda - \lambda_0; \bar{g}_2, \bar{g}_3) - \frac{\bar{C}_2}{3})\right). \tag{5.31}$$

[2] Equivalently, one can apply a similar transformation on the variables such that $\frac{\bar{x}-\bar{x}_4}{\bar{x}-\bar{x}_1} = \frac{\bar{x}_3-\bar{x}_4}{\bar{x}_3-\bar{x}_1} y_\theta^2$ and obtain the same analytical result for the solution of the angular equation where the transformation is valid when $\bar{x}_4 \leq \bar{x} \leq \bar{x}_3$.

We further remark that, here

$$\bar{C}_0 = C_0|_{\bar{E}=1}\,, \quad \bar{C}_1 = C_1|_{\bar{E}=1}\,, \quad \bar{C}_2 = C_2|_{\bar{E}=1}\,, \quad \bar{C}_3 = C_3|_{\bar{E}=1}\,. \tag{5.32}$$

In addition, one can also consider the special case where $\bar{E}=1$ and $a=0$. For this special case, the angular equation becomes a second order polynomial which can be solved as

$$\theta(\lambda) = \arccos\left[\frac{2\ell\bar{L}}{\frac{K}{m^2}+3\ell^2} + \sqrt{\tilde{C}}\sin\left(\sqrt{\frac{K}{m^2}+3\ell^2}\,(\lambda-\lambda_0)\right)\right] \tag{5.33}$$

where we also identify

$$\tilde{C} = \frac{1}{\left(\frac{K}{m^2}+3\ell^2\right)^2}\left[\left(\frac{K}{m^2}-\ell^2-\bar{L}^2\right)\left(\frac{K}{m^2}+3\ell^2\right)+4\ell^2\bar{L}^2\right] \tag{5.34}$$

provided that $\tilde{C}>0$.

## 5.2 $r$-motion

On the other hand, the transformation (3.13) on the time variable brings the radial equation (3.8) into

$$\left(\frac{dr}{d\lambda}\right)^2 = N_0 + N_1 r + N_2 r^2 + N_3 r^3 + N_4 r^4 =: P_r(r), \tag{5.35}$$

where

$$N_4 = \bar{E}^2 - 1, \tag{5.36}$$

$$N_3 = 2(M - \bar{E}\bar{q}Q), \tag{5.37}$$

$$\begin{aligned} N_2 &= a^2(2\bar{E}^2-1) + \ell^2(2\bar{E}^2+1) + Q^2(\bar{q}^2-1) - 2a\bar{E}\bar{L} - \frac{K}{m^2}, \\ &= -\widetilde{K} + a^2(\bar{E}^2-1) + 2\ell^2\bar{E}^2 + Q^2(\bar{q}^2-1) - \bar{L}^2, \end{aligned} \tag{5.38}$$

$$N_1 = 2\bar{q}Q\left(a\bar{L} - (\ell^2+a^2)\bar{E}\right) + \frac{2MK}{m^2}, \tag{5.39}$$

and

$$N_0 = \left((\ell^2+a^2)\bar{E} - a\bar{L}\right)^2 - \left(a^2-\ell^2+Q^2\right)\frac{K}{m^2}. \tag{5.40}$$

If one performs the transformation (for $\bar{E} \neq 1$)

$$r = \frac{\beta_3}{\left(4v - \frac{\beta_2}{3}\right)} + r_1 \tag{5.41}$$

the equation (5.35) can be brought into the standard Weierstrass form

$$\left(\frac{dv}{d\lambda}\right)^2 = 4v^3 - h_2 v - h_3, \tag{5.42}$$

where

$$\beta_1 = N_3 + 4N_4 r_1, \tag{5.43}$$

$$\beta_2 = N_2 + 3N_3 r_1 + 6N_4 r_1^2, \tag{5.44}$$

$$\beta_3 = N_1 + 2N_2 r_1 + 3N_3 r_1^2 + 4N_4 r_1^3, \tag{5.45}$$

with

$$h_2 = \frac{1}{12}\left(\beta_2^2 - 3\beta_1\beta_3\right), \qquad h_3 = \frac{1}{8}\left(\frac{\beta_1\beta_2\beta_3}{6} - \frac{N_4\beta_3^2}{2} - \frac{\beta_2^3}{27}\right), \tag{5.46}$$

whose solution can again be given by Weierstrass $\wp$ function

$$v(\lambda) = \wp(\lambda - \lambda_0; h_2, h_3), \tag{5.47}$$

so that the solution for $r$ can be written as

$$r = \frac{\beta_3}{\left(4\wp(\lambda - \lambda_0; h_2, h_3) - \frac{\beta_2}{3}\right)} + r_1, \tag{5.48}$$

where we have assumed that $P_r(r)$ has at least two real roots (Here $r_1$ is assumed to be one real root of $P_r(r)$).
As in the angular motion, if one considers that the radial polynomial $P_r(r)$ has 4 distinct real roots $r_1, r_2, r_3, r_4$ ordered as $r_4 < r_3 < r_2 < r_1$, one can alternatively express the solutions in terms of Jacobian Elliptic functions. If one performs the similar transformations done in the angular case, one can end up with the following solutions: For the orbits where $\bar{E} > 1$, the solution reads

$$F(y_r, k_r) = \sqrt{N_4\left(r_1 - r_3\right)\left(r_2 - r_4\right)}\frac{(\lambda - \lambda_0)}{2}, \tag{5.49}$$

where we have affected the transformation

$$\frac{r-r_1}{r-r_2}=\frac{r_1-r_4}{r_2-r_4}y_r^2 \tag{5.50}$$

with

$$k_r^2=\frac{(r_1-r_4)(r_2-r_3)}{(r_1-r_3)(r_2-r_4)} \tag{5.51}$$

while for the orbits where $\bar{E}<1$, the solution can similarly be expressed as

$$F(y_r,\bar{k}_r)=\sqrt{-N_4\,(r_1-r_3)\,(r_2-r_4)}\frac{(\lambda-\lambda_0)}{2}, \tag{5.52}$$

where in that case, the transformation

$$\frac{r-r_2}{r-r_3}=\frac{r_1-r_2}{r_1-r_3}y_r^2 \tag{5.53}$$

is valid with

$$\bar{k}_r^2=\frac{(r_1-r_2)(r_3-r_4)}{(r_1-r_3)(r_2-r_4)}. \tag{5.54}$$

Interestingly, for the special case where $P_r(r)$ has a double real root such that $r_1=r_2=r_s$, the radial polynomial can be put into the form (with $\bar{E}\neq 1$) [16]

$$P_r(r)=(r-r_s)^2\left\{(\bar{E}^2-1)r^2+2rr_s\left(\bar{E}^2-1+\frac{M-\bar{q}Q\bar{E}}{r_s}\right)+\frac{N_0}{r_s^2}\right\}. \tag{5.55}$$

At this stage, we can affect the transformation

$$\rho=\frac{1}{r-r_s}, \tag{5.56}$$

to obtain (5.35) in the following form:

$$\left(\frac{d\rho}{d\lambda}\right)^2=\alpha+\beta\rho+\gamma\rho^2, \tag{5.57}$$

where

$$\alpha=N_4=\bar{E}^2-1, \tag{5.58}$$

$$\beta=4r_s(\bar{E}^2-1)+2(M-\bar{E}\bar{q}Q), \tag{5.59}$$

$$\gamma = 3r_s^2(\bar{E}^2 - 1) + 2r_s(M - \bar{E}\bar{q}Q) + \frac{N_0}{r_s^2}. \tag{5.60}$$

The solution of the equation (5.57) can be obtained for three different cases, namely for the cases $\gamma > 0$, $\gamma = 0$ and $\gamma < 0$. For $\gamma = 0$, the solution can be expressed as

$$\lambda - \lambda_0 = \mp \frac{2\sqrt{\alpha + \beta\rho}}{\beta}, \tag{5.61}$$

for $\gamma > 0$, the solution can be given by

$$\lambda - \lambda_0 = \mp \frac{1}{\sqrt{\gamma}} \ln \left| \rho + \frac{\beta}{2\gamma} + \sqrt{\rho^2 + \frac{\beta}{\gamma}\rho + \frac{\alpha}{\gamma}} \right|, \tag{5.62}$$

while for $\gamma < 0$ the solution reads

$$\lambda - \lambda_0 = \mp \frac{1}{\sqrt{-\gamma}} \arcsin \left( \frac{2\gamma\rho + \beta}{\sqrt{\beta^2 - 4\gamma\alpha}} \right). \tag{5.63}$$

Interestingly for $\bar{E} = 1$, $P_r(r)$ turns into a third order polynomial such that the transformation

$$r = \frac{\bar{N}_3}{\left(4v - \frac{\bar{N}_2}{3}\right)} \tag{5.64}$$

brings the radial equation into standard Weierstrass-$\wp$ form

$$\left(\frac{dv}{d\lambda}\right)^2 = 4v^3 - \bar{h}_2 v - \bar{h}_3 \tag{5.65}$$

where in that case we identify

$$\bar{h}_2 = \frac{1}{4}\left(\frac{\bar{N}_2^2}{3} - \bar{N}_1\bar{N}_3\right), \tag{5.66}$$

$$\bar{h}_3 = \frac{1}{8}\left(\frac{\bar{N}_1\bar{N}_2\bar{N}_3}{6} - \frac{\bar{N}_0\bar{N}_3^2}{2} - \frac{\bar{N}_2^3}{27}\right) \tag{5.67}$$

with

$$\bar{N}_0 = N_0|_{\bar{E}=1}\,, \quad \bar{N}_1 = N_1|_{\bar{E}=1}\,, \quad \bar{N}_2 = N_2|_{\bar{E}=1}\,, \quad \bar{N}_3 = N_3|_{\bar{E}=1}\,. \tag{5.68}$$

Then, for $\bar{E} = 1$, the solution reads

$$r(\lambda) = \frac{\bar{N}_3}{4\wp(\lambda - \lambda_0; \bar{h}_2, \bar{h}_3) - \frac{\bar{N}_2}{3}}. \tag{5.69}$$

## 5.3 $t$-motion

To obtain the solution of the equation (3.16), we recall that it can be written in differential form as

$$dt = dI^{(t)}_{\theta,1} + dI^{(t)}_{\theta,2} + dI^{(t)}_{r} \tag{5.70}$$

where the integration yields

$$t - t_0 = I^{(t)}_{\theta,1} + I^{(t)}_{\theta,2} + I^{(t)}_{r}. \tag{5.71}$$

Here

$$I^{(t)}_{\theta,1} = a\bar{L}\int_{\theta_0}^{\theta(\lambda)} \frac{d\theta}{\sqrt{P_\theta(\theta)}} = a\bar{L}(\lambda - \lambda_0) \tag{5.72}$$

where we have integrated (3.15), taking the + sign only. The second expression $I^{(t)}_{\theta,2}$ can be written as

$$\begin{aligned} I^{(t)}_{\theta,2} &= -2\ell\bar{L}\int_{\theta_0}^{\theta(\lambda)} \frac{\cos\theta}{\sin^2\theta\sqrt{P_\theta(\theta)}}\,d\theta - a^2\bar{E}\int_{\theta_0}^{\theta(\lambda)} \frac{\sin^2\theta}{\sqrt{P_\theta(\theta)}}\,d\theta \\ &\quad +4a\ell\bar{E}\int_{\theta_0}^{\theta(\lambda)} \frac{\cos\theta}{\sqrt{P_\theta(\theta)}}\,d\theta - 4\ell^2\bar{E}\int_{\theta_0}^{\theta(\lambda)} \frac{\cos^2\theta}{\sin^2\theta\sqrt{P_\theta(\theta)}}\,d\theta. \end{aligned} \tag{5.73}$$

The integration $I^{(t)}_{\theta,2}$ can be accomplished first by taking $x = \cos\theta$ and next by making further transformation

$$x = \frac{\alpha_3}{\left(4y - \frac{\alpha_2}{3}\right)} + x_\theta, \tag{5.74}$$

where $x_\theta$ is one real root of the polynomial equation (5.1) and $\alpha_2$ and $\alpha_3$ are defined as in (5.11) and (5.12) respectively. With the additional transforma-

tion $\wp(s) = y$, integrations with respect to variable $s$ yield

$$
\begin{aligned}
I^{(t)}_{\theta,2} &= \left(a^2\bar{E}^2(x_\theta^2-1) + 4a\ell\bar{E}x_\theta - \frac{2x_\theta\ell}{1-x_\theta^2}\left(2\ell\bar{E}x_\theta + \bar{L}\right)\right)(\lambda-\lambda_0) \\
&\quad -2\ell\sum_{i=1}^{2}\sum_{j=1}^{2}\frac{(\bar{L}G_i + 2\ell\bar{E}\bar{G}_i)}{\wp'(a_{ij})}\left(\zeta(a_{ij})(\lambda-\lambda_0) + \ln\frac{\sigma(s-a_{ij})}{\sigma(s_0-a_{ij})}\right) \\
&\quad +a\bar{E}\left(\frac{ax_\theta}{2} + \ell\alpha_3\right)\sum_{i=1}^{2}\frac{1}{\wp'(b_{1i})}\left(\zeta(b_{1i})(\lambda-\lambda_0) + \ln\frac{\sigma(s-b_{1i})}{\sigma(s_0-b_{1i})}\right) \\
&\quad -\frac{a^2\bar{E}\alpha_3^2}{16}\sum_{i=1}^{2}\frac{1}{\wp'^2(b_{1i})}(\lambda-\lambda_0)\left(\wp(b_{1i}) + \frac{\wp''(b_{1i})}{\wp'(b_{1i})}\right) \qquad (5.75) \\
&\quad -\frac{a^2\bar{E}\alpha_3^2}{16}\sum_{i=1}^{2}\frac{1}{\wp'^2(b_{1i})}\left(\zeta(s-b_{1i}) + \frac{\wp''(b_{1i})}{\wp'(b_{1i})}\ln\frac{\sigma(s-b_{1i})}{\sigma(s_0-b_{1i})} - \zeta_0^{(i)}\right).
\end{aligned}
$$

Here we identify $\wp(a_{ij}) = a_i$ and $\wp(b_{1i}) = b_1 = \frac{\alpha_2}{12}$ $(i = 1, 2)$ with

$$
a_1 = \frac{\bar{c}}{4(1-x_\theta)}, \qquad a_2 = -\frac{\bar{c}}{4(1+x_\theta)}, \qquad (5.76)
$$

where

$$
\bar{c} = \alpha_3 + \frac{\alpha_2}{3}(1-x_\theta). \qquad (5.77)
$$

Also,

$$
G_1 = \frac{\alpha_3}{8(1-x_\theta^2)}\left(\frac{(1-3x_\theta^2)}{(1-x_\theta)} + \frac{1}{3\bar{c}}\left(3\alpha_3x_\theta - \alpha_2\right)\right), \qquad (5.78)
$$

$$
G_2 = \frac{\alpha_3}{8(1-x_\theta^2)}\left(\frac{(1-3x_\theta^2)}{(1+x_\theta)} - \frac{1}{3\bar{c}}\left(3\alpha_3x_\theta - \alpha_2\right)\right), \qquad (5.79)
$$

$$
\bar{G}_1 = \frac{\alpha_3}{4(1-x_\theta^2)}\left(\frac{x_\theta}{(1-x_\theta)} + \frac{1}{3\bar{c}}(x_\theta\alpha_2 - \alpha_3))\right), \qquad (5.80)
$$

$$
\bar{G}_2 = \frac{\alpha_3}{4(1-x_\theta^2)}\left(\frac{x_\theta}{(1+x_\theta)} - \frac{1}{3\bar{c}}(x_\theta\alpha_2 - \alpha_3))\right). \qquad (5.81)
$$

Next, we consider the radial integral

$$
I^{(t)}_r = \int_{r_0}^{r(\lambda)}\left(\bar{E}(r^2+a^2+\ell^2) - a\bar{L} - \bar{q}Qr\right)\frac{(r^2+a^2+\ell^2)}{\Delta\sqrt{P_r(r)}}dr. \qquad (5.82)
$$

The radial integrals can be evaluated by a similar transformation such that

$$r = \frac{\beta_3}{(4v - \frac{\beta_2}{3})} + r_1 \tag{5.83}$$

where $r_1$ is again assumed to be one real root of $P_r(r)$. Next taking $v = \wp(s)$, the integration yields

$$\begin{aligned} I_r^{(t)} &= \left[\bar{E}(r_1^2+\ell^2+a^2)^2 - \bar{q}Q(r_1^2+\ell^2+a^2)r_1 - a\bar{L}(r_1^2+1)\right]\frac{(\lambda-\lambda_0)}{\Delta(r_1)} \\ &+ \sum_{i=1}^{3}\sum_{j=1}^{2}\frac{(\bar{E}\omega_i - \bar{q}Q\bar{\omega}_i)}{\wp'(v_{ij})}\left(\zeta(v_{ij})(\lambda-\lambda_0) + \ln\frac{\sigma(s-v_{ij})}{\sigma(s_0-v_{ij})}\right) \\ &- \frac{\bar{E}\beta_3^2}{16}\sum_{j=1}^{2}\frac{1}{\wp'^2(v_{3j})}\left\{(\lambda-\lambda_0)\left(\wp(v_{3j}) + \frac{\wp''(v_{3j})}{\wp'(v_{3j})}\right)\right. \\ &\left. + \frac{\wp''(v_{3j})}{\wp'(v_{3j})}\ln\frac{\sigma(s-v_{3j})}{\sigma(s_0-v_{3j})} + \zeta(s-v_{3j}) - \zeta_0^{(j)}\right\} \\ &+ \sum_{i=1}^{2}\sum_{j=1}^{2}\frac{1}{\wp'(v_{ij})}\left(\zeta(v_{ij})(\lambda-\lambda_0) + \ln\frac{\sigma(s-v_{ij})}{\sigma(s_0-v_{ij})}\right)\times \\ &\left(\left(2\bar{E}(\ell^2+a^2) - a\bar{L}\right)\tilde{\omega}_i - \bar{q}Q(\ell^2+a^2)\hat{\omega}_i + (\ell^2+a^2)\left(\bar{E}(\ell^2+a^2) - a\bar{L}\right)\breve{\omega}_i\right). \end{aligned} \tag{5.84}$$

Here $\wp(v_{ij}) = v_i$ and $\wp(v_{3j}) = v_3 = \frac{\beta_2}{12}$ $(i = 1, 2)$ with

$$v_1 = \frac{1}{4\Delta(r_1)}\left(\left(\frac{\Delta(r_1)\beta_2}{3} - r_1 + M\beta_3\right) - \sqrt{(r_1 - M\beta_3)^2 - \Delta(r_1)\beta_3^2}\right) \tag{5.85}$$

and

$$v_2 = \frac{1}{4\Delta(r_1)}\left(\left(\frac{\Delta(r_1)\beta_2}{3} - r_1 + M\beta_3\right) + \sqrt{(r_1 - M\beta_3)^2 - \Delta(r_1)\beta_3^2}\right). \tag{5.86}$$

We also identify

$$\omega_1 = -\frac{\left[r_1(r_1 - M\beta_3) - \beta_3\Delta(r_1) + 2r_1\Delta(r_1)(v_2 - v_1)\right]^4}{16\Delta^3(r_1)(v_2 - v_1)\left[r_1 - M\beta_3 + 2\Delta(r_1)(v_2 - v_1)\right]^2}, \tag{5.87}$$

$$\omega_2 = \frac{\left[r_1(r_1 - M\beta_3) - \beta_3\Delta(r_1) - 2r_1\Delta(r_1)(v_2 - v_1)\right]^4}{16\Delta^3(r_1)(v_2 - v_1)\left[r_1 - M\beta_3 - 2\Delta(r_1)(v_2 - v_1)\right]^2}, \tag{5.88}$$

$$\bar{\omega}_1 = -\frac{\left[r_1(r_1 - M\beta_3) - \beta_3\Delta(r_1) + 2r_1\Delta(r_1)(v_2 - v_1)\right]^3}{16\Delta^3(r_1)(v_2 - v_1)\left[r_1 - M\beta_3 + 2\Delta(r_1)(v_2 - v_1)\right]}, \tag{5.89}$$

$$\bar{\omega}_2 = \frac{\left[r_1(r_1 - M\beta_3) - \beta_3\Delta(r_1) - 2r_1\Delta(r_1)(v_2 - v_1)\right]^3}{16\Delta^3(r_1)(v_2 - v_1)\left[r_1 - M\beta_3 - 2\Delta(r_1)(v_2 - v_1)\right]}, \tag{5.90}$$

$$\omega_3 = \beta_3 r_1 - \frac{(r_1 - M\beta_3)}{2}, \qquad \bar{\omega}_3 = \frac{\beta_3}{4}, \tag{5.91}$$

$$\tilde{\omega}_1 = -\frac{\left[r_1(r_1 - M\beta_3) - \beta_3\Delta(r_1) + 2r_1\Delta(r_1)(v_2 - v_1)\right]^2}{16\Delta^3(r_1)(v_2 - v_1)}, \tag{5.92}$$

$$\tilde{\omega}_2 = \frac{\left[r_1(r_1 - M\beta_3) - \beta_3\Delta(r_1) - 2r_1\Delta(r_1)(v_2 - v_1)\right]^2}{16\Delta^3(r_1)(v_2 - v_1)}, \tag{5.93}$$

$$\hat{\omega}_1 = \frac{1}{\Delta(r_1)(v_1 - v_2)}\left(v_1 - \frac{\beta_2}{12}\right)\left(r_1\left(v_1 - \frac{\beta_2}{12}\right) + \frac{\beta_3}{4}\right), \tag{5.94}$$

$$\hat{\omega}_2 = \frac{1}{\Delta(r_1)(v_2 - v_1)}\left(v_2 - \frac{\beta_2}{12}\right)\left(r_1\left(v_2 - \frac{\beta_2}{12}\right) + \frac{\beta_3}{4}\right), \tag{5.95}$$

$$\check{\omega}_1 = \frac{1}{\Delta(r_1)(v_1 - v_2)}\left(v_1 - \frac{\beta_2}{12}\right)^2 \tag{5.96}$$

and

$$\check{\omega}_2 = \frac{1}{\Delta(r_1)(v_2 - v_1)}\left(v_2 - \frac{\beta_2}{12}\right)^2. \tag{5.97}$$

## 5.4 $\varphi$-motion

Similarly, the equation (3.17) can be written in differential form as

$$d\varphi = dI_\theta^{(\varphi)} + dI_r^{(\varphi)} \tag{5.98}$$

upon integration which gives

$$\varphi - \varphi_0 = I_\theta^{(\varphi)} + I_r^{(\varphi)}. \tag{5.99}$$

The angular integral

$$I_\theta^{(\varphi)} = \int \frac{\left(\bar{L} - \bar{E}(a\sin^2\theta - 2\ell\cos\theta)\right)}{\sin^2\theta\sqrt{P_\theta(\theta)}}d\theta \tag{5.100}$$

can be accomplished by making the transformation

$$\cos\theta = \frac{\alpha_3}{\left(4\wp(s) - \frac{\alpha_2}{3}\right)} + x_\theta \tag{5.101}$$

such that it yields the solution

$$\begin{aligned} I_\theta^{(\varphi)} &= \left(\frac{(\bar{L} + 2\ell\bar{E}x_\theta)}{(1-x_\theta^2)} - a\bar{E}\right)(\lambda - \lambda_0) \\ &+ \sum_{i=1}^{2}\sum_{j=1}^{2} \frac{(\bar{L}\bar{G}_i + 2\ell\bar{E}G_i)}{\wp'(a_{ij})}\left(\zeta(a_{ij})(\lambda-\lambda_0) + \ln\frac{\sigma(s-a_{ij})}{\sigma(s_0-a_{ij})}\right) \end{aligned} \tag{5.102}$$

where $G_i$ and $\bar{G}_i$ are defined through (5.78)-(5.81).
On the other hand, the radial integral

$$I_r^{(\varphi)} = \int_{r_0}^{r(\lambda)} \frac{a\left((r^2+a^2+\ell^2) - a\bar{L} - \bar{q}Qr\right)}{\Delta\sqrt{P_r(r)}} dr \tag{5.103}$$

can be calculated by affecting the transformation

$$r = \frac{\beta_3}{(4\wp(s) - \frac{\beta_2}{3})} + r_1 \tag{5.104}$$

that yields

$$\begin{aligned} I_r^{(\varphi)} &= \frac{a(r_1^2 - \bar{q}Qr_1 + a^2 + \ell^2 - a\bar{L})}{\Delta}(\lambda - \lambda_0) \\ &+ \sum_{i=1}^{2}\sum_{j=1}^{2} \frac{a(\tilde{\omega}_i - \bar{q}Q\hat{\omega}_i + (a^2+\ell^2-a\bar{L})\check{\omega}_i)}{\wp'(v_{ij})}\left(\zeta(v_{ij})(\lambda-\lambda_0) + \ln\frac{\sigma(s-v_{ij})}{\sigma(s_0-v_{ij})}\right) \end{aligned} \tag{5.105}$$

where $\tilde{\omega}_i$, $\hat{\omega}_i$ and $\check{\omega}_i$ are identified through (5.92)-(5.97).

# 6 Discussion of the orbits and observables

In this section, we investigate possible three dimensional orbits by plotting them for fixed energy, angular momentum and spacetime parameters. In addition, we also calculate the observables of the bound orbits and express them in terms of the elliptic functions.

We first examine the orbits with respect to value of the energy parameter. In Figures 10 and 11, orbits are plotted for $\bar{E} < 1$. It can be seen that for $\bar{E} < 1$, there may exist one bound or two bound orbits. In Figure 10, for the value of NUT parameter $\ell = 0.1$, we obtain two bound orbits ($P_r(r)$ has four real zeros), while in figure 11, for $\ell = 0.3$ (i.e NUT parameter is slightly increased) there exists one bound orbit ($P_r(r)$ has two real zeros).

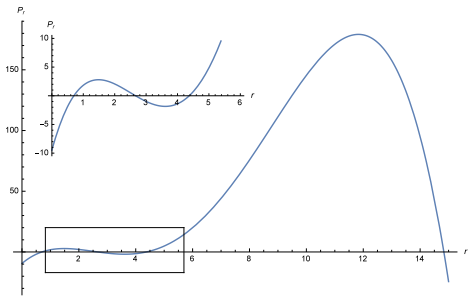

(a) The graph of $P_r(r)$

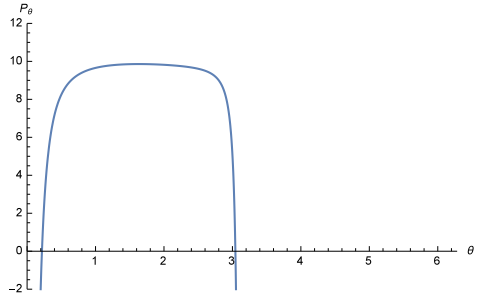

(b) The graph of $P_\theta(\theta)$

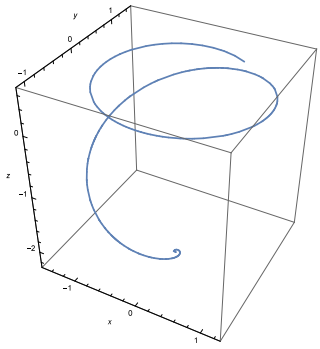

(c) 3D-bound orbit with $\bar{E} < 1$

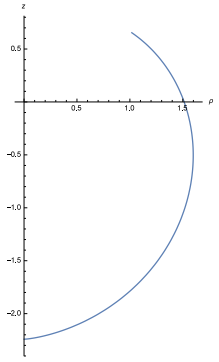

(d) $r$-$\theta$ plane

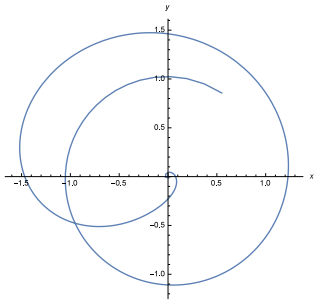

(e) Projection onto $xy$-plane

Figure 10: The plots are obtained for the parameters $M = 1$, $a = 0.9$, $K = 10$, $Q = 0.4$, $\bar{q} = 0.3$, $\bar{L} = 0.5$, $\bar{E} = 0.96$, $\ell = 0.1$ and $m = 1$. Here $\rho^2 = x^2 + y^2$. There exist two bound orbits.

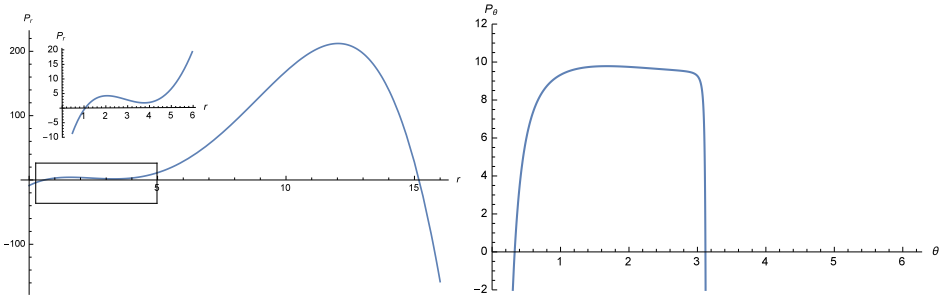

(a) The graph of $P_r(r)$ (b) The graph of $P_\theta(\theta)$

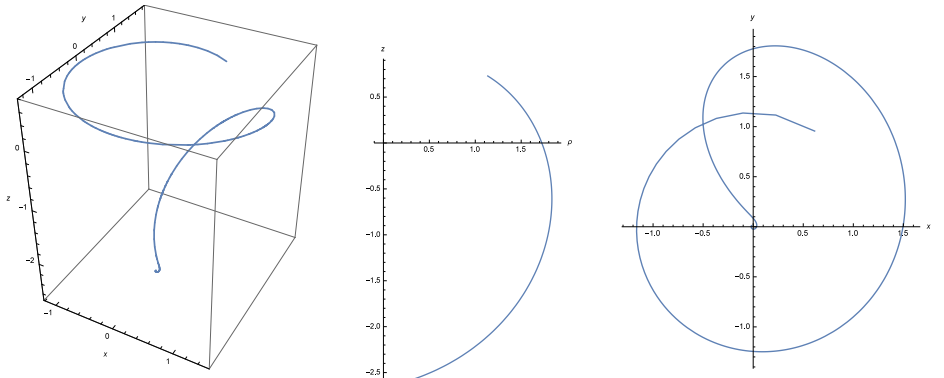

(c) 3D-bound orbit with $\bar{E} < 1$ (d) $r$-$\theta$ plane (e) Projection onto $xy$-plane

Figure 11: The plots are obtained for the parameters $M = 1$, $a = 0.9$, $K = 10$, $Q = 0.4$, $\bar{q} = 0.3$, $\bar{L} = 0.5$, $\bar{E} = 0.96$, $\ell = 0.3$ and $m = 1$. Here $\rho^2 = x^2 + y^2$. There exists one bound orbit.

On the other hand, for $\bar{E} > 1$, one can get one bound and two flyby obits ($P_r(r)$ has four real zeros) or two flyby orbits ($P_r(r)$ has two real zeros) or transit orbits ($P_r(r)$ has no real zeros). In Figures 12 and 13, 3D-flyby orbits are obtained for different values of the NUT parameter, while in Figures 14 and 15, 3D-bound orbits (with $\bar{E} > 1$) are realized similarly for different values of gravitomagnetic monopole moment $\ell$.

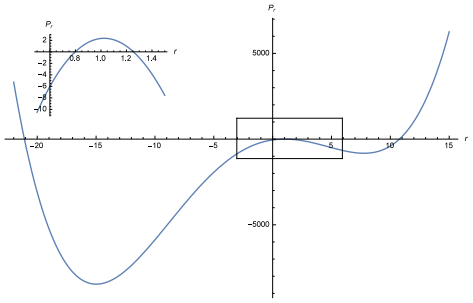

(a) The graph of $P_r(r)$

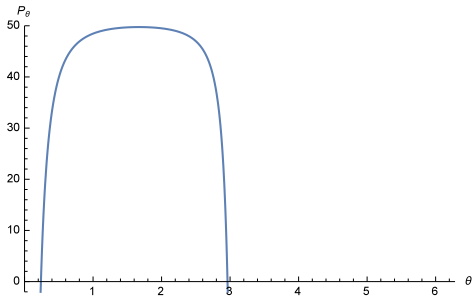

(b) The graph of $P_\theta(\theta)$

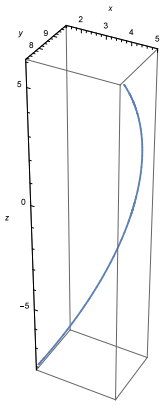

(c) 3D-flyby orbit for $r > r_1$ with $\bar{E} > 1$.

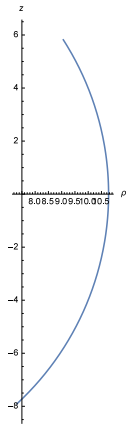

(d) $r$-$\theta$ plane

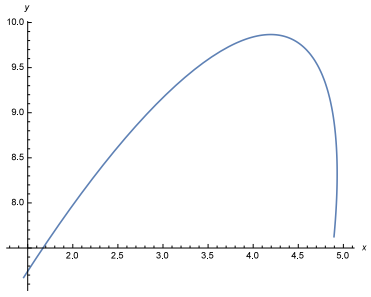

(e) Projection onto $xy$-plane

Figure 12: The plots are obtained for the parameters $M = 1$, $a = 0.9$, $K = 50$, $Q = 0.4$, $\bar{q} = 0.3$, $\bar{L} = 1.5$, $\bar{E} = 1.1$, $\ell = 0.1$ and $m = 1$. Here $\rho^2 = x^2 + y^2$ and $r_1 = 10.768$ is one real root of $P_r(r)$. There exists one bound orbit and two flyby orbits.

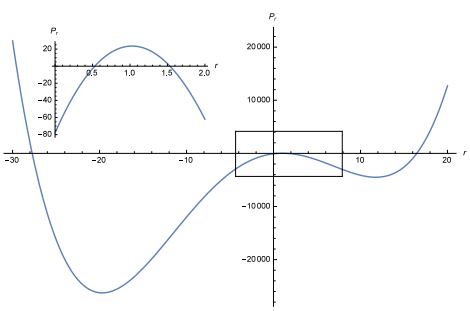


(a) The graph of $P_r(r)$

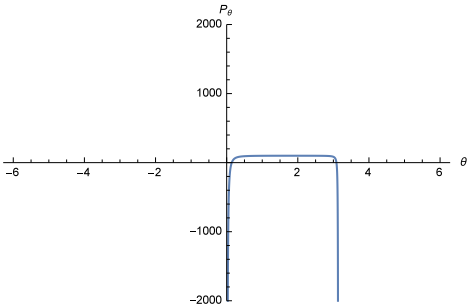


(b) The graph of $P_\theta(\theta)$

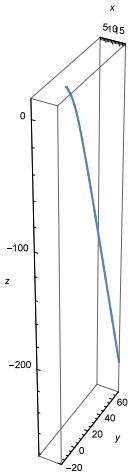


(c) 3D-flyby orbit for $r > r_1$ with $\bar{E} > 1$.

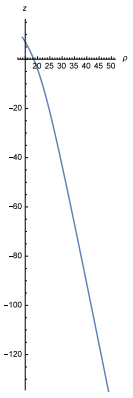


(d) $r$-$\theta$ plane

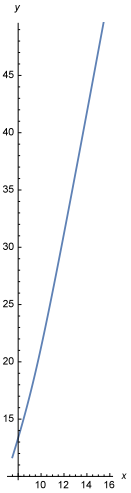


(e) Projection onto $xy$-plane

Figure 13: The plots are obtained for the parameters $M = 1$, $a = 0.9$, $K = 100$, $Q = 0.1$, $\bar{q} = 0.3$, $\bar{L} = 1$, $\bar{E} = 1.1$, $\ell = 0.2$ and $m = 1$. Here $\rho^2 = x^2 + y^2$ and $r_1 = 16.473$ is one real root of $P_r(r)$. There exists one bound orbit and two flyby orbits.

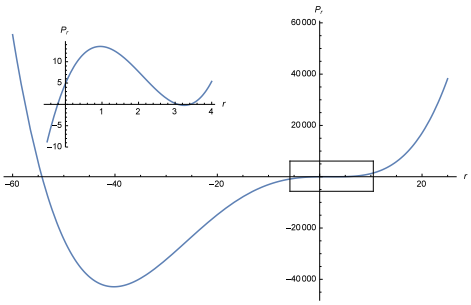

(a) The graph of $P_r(r)$

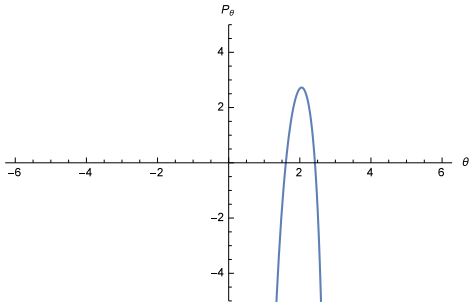

(b) The graph of $P_\theta(\theta)$

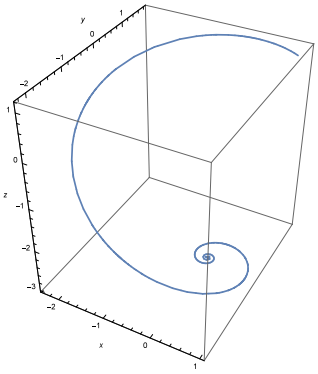

(c) 3D-bound orbit with $\bar{E} > 1$

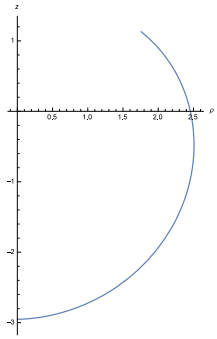

(d) $r$-$\theta$ plane

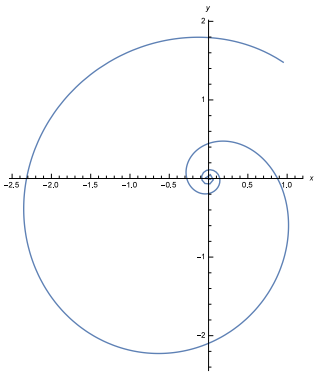

(e) Projection onto $xy$-plane

Figure 14: The plots are obtained for the parameters $M = 1$, $a = 0.9$, $K = 10$, $Q = 0.1$, $\bar{q} = 0.3$, $\bar{L} = 4$, $\bar{E} = 1.02$, $\ell = 1$ and $m = 1$. Here $\rho^2 = x^2 + y^2$. There exists one bound orbit and two flyby orbits.

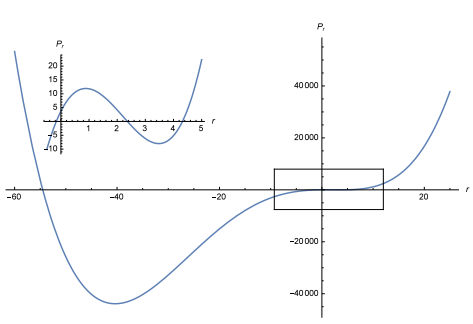

(a) The graph of $P_r(r)$

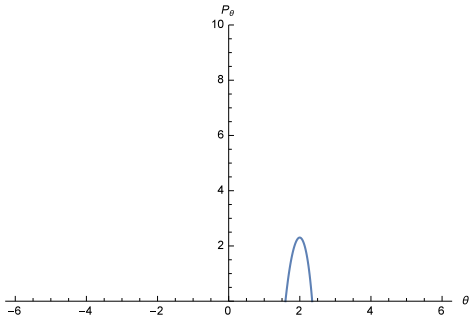

(b) The graph of $P_\theta(\theta)$

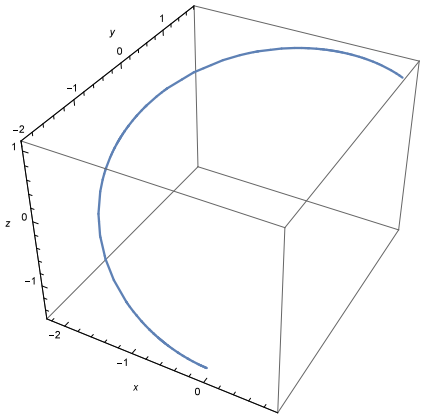

(c) 3D-bound orbit with $\bar{E} > 1$

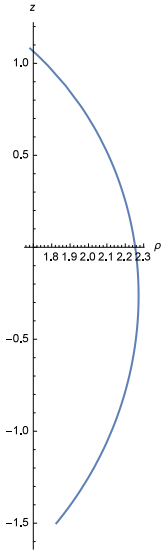

(d) $r$-$\theta$ plane

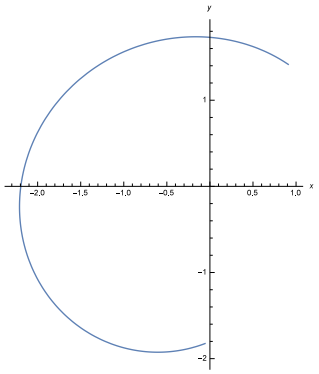

(e) Projection onto $xy$-plane

Figure 15: The plots are obtained for the parameters $M = 1$, $a = 0.9$, $K = 10$, $Q = 0.1$, $\bar{q} = 0.3$, $\bar{L} = 4$, $\bar{E} = 1.02$, $\ell = 0.9$ and $m = 1$. Here $\rho^2 = x^2 + y^2$. There exists one bound orbit and two flyby orbits.

Finally, for $\bar{E} = 1$ the possible orbit types can be one bound and one flyby ($P_r(r)$ has three real zeros) or one flyby orbit ($P_r(r)$ has only one real zero). In Figure 16, we give an example of flyby orbit while in Figure 17, we exhibit 3D-bound orbit for $\bar{E} = 1$ (for the fixed value of the NUT parameter but different values of the test particle charge $\bar{q}$).

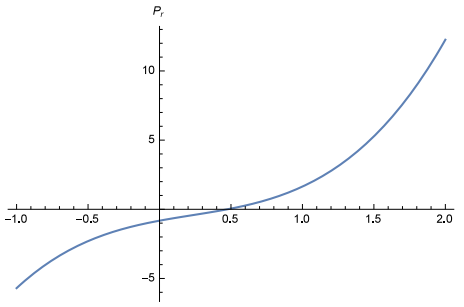


(a) The graph of $P_r(r)$

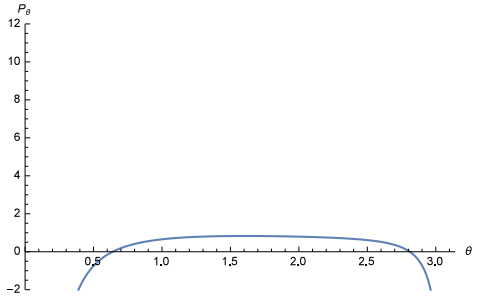


(b) The graph of $P_\theta(\theta)$

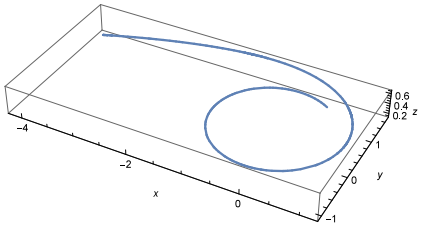


(c) 3D-flyby orbit with $\bar{E} = 1$

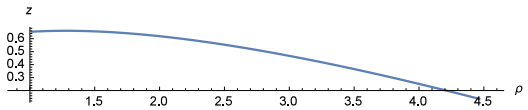


(d) $r$-$\theta$ plane

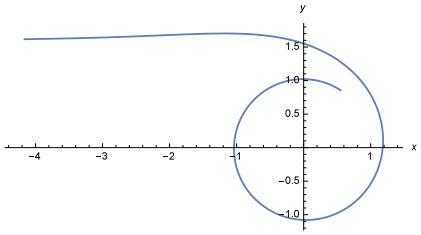


(e) Projection onto $xy$-plane

Figure 16: The plots are obtained for the parameters $M = 1$, $a = 0.9$, $K = 1$, $Q = 0.4$, $\bar{q} = 0.3$, $\bar{L} = 0.5$, $\bar{E} = 1$, $\ell = 0.1$ and $m = 1$. Here $\rho^2 = x^2 + y^2$. There exists one flyby orbit.

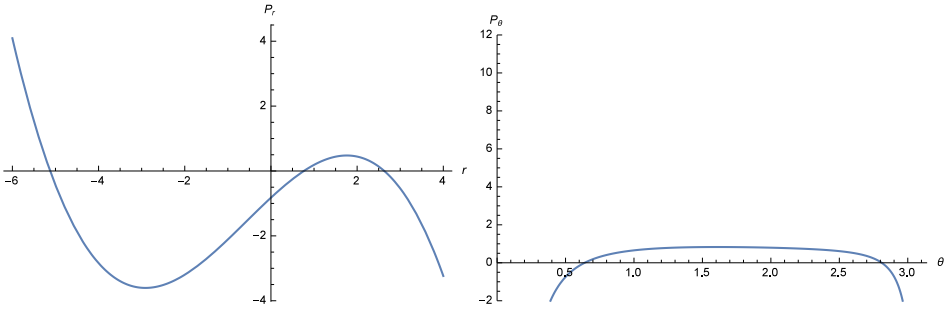


(a) The graph of $P_r(r)$ (b) The graph of $P_\theta(\theta)$

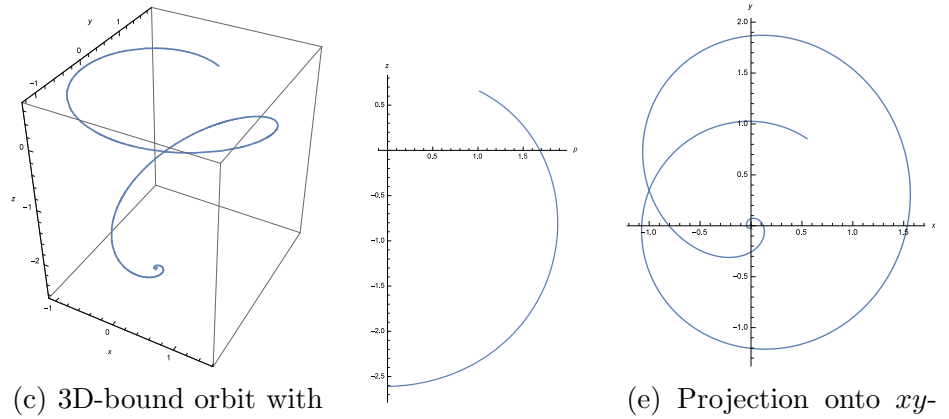

(c) 3D-bound orbit with $\bar{E} = 1$ (d) $r$-$\theta$ plane (e) Projection onto $xy$-plane

Figure 17: The plots are obtained for the parameters $M = 1$, $a = 0.9$, $K = 1$, $Q = 0.4$, $\bar{q} = 2.6$, $\bar{L} = 0.5$, $\bar{E} = 1$, $\ell = 0.1$ and $m = 1$. Here $\rho^2 = x^2 + y^2$. There exists one bound orbit.

Next, to obtain the observables for a charged particle in Kerr-Newman-Taub-NUT spacetime, we assume that the particle makes a bound motion in $r$ and $\theta$ coordinates. Considering that motion in $r$-coordinate is bounded in the interval $r_2 \leq r \leq r_1$, one can calculate the fundamental period $\Lambda_r$ for the radial motion as

$$\Lambda_r = 2\int_{r_2}^{r_1} \frac{dr}{\sqrt{P_r(r)}} = 2\int_{v_0}^{\infty} \frac{dv}{\sqrt{P_3(v)}} \tag{6.1}$$

where $P_3(v) = 4v^3 - h_2 v - h_3$ with $h_2$ and $h_3$ introduced in (5.46). The integral can be accomplished via the transformation

$$\xi_r = \frac{1}{\kappa_r}\left(\frac{e_2 - e_3}{v - e_3}\right)^{1/2} \tag{6.2}$$

where $e_1$, $e_2$ and $e_3$ correspond to the roots of the polynomial $P_3(v) = 0$ with $\kappa_r^2 = \frac{e_2 - e_3}{e_1 - e_3}$. We also choose $v_0 = e_1$. Then one obtains the radial period as

$$\Lambda_r = \frac{2}{\sqrt{e_1 - e_3}} K(\kappa_r) \tag{6.3}$$

where $K(\kappa_r)$ denotes the complete elliptic function with modulus $\kappa_r$.
Similarly, if one considers that the angular motion is also bounded in the angular interval $\theta_2 \leq \theta \leq \theta_1$, one can evaluate the fundamental period $\Lambda_\theta$ for the angular motion in the form

$$\Lambda_\theta = 2 \int_{\theta_2}^{\theta_1} \frac{d\theta}{\sqrt{P_\theta(\theta)}} = \frac{2}{\sqrt{\bar{e}_1 - \bar{e}_3}} K(\kappa_\theta), \tag{6.4}$$

where in this case $\bar{e}_1$, $\bar{e}_2$, $\bar{e}_3$ correspond to roots of the polynomial $P_3(y) = 4y^3 - g_2 y - g_3$. Here, $g_2$ and $g_3$ are expressed in (5.15) and (5.16) respectively and $\kappa_\theta^2 = \frac{\bar{e}_2 - \bar{e}_3}{\bar{e}_1 - \bar{e}_3}$. Similarly $K(\kappa_\theta)$ describes the complete elliptic function with modulus $\kappa_\theta$. Then one can also evaluate the corresponding angular frequencies

$$\Upsilon_r = \frac{2\pi}{\Lambda_r} = \frac{\pi \sqrt{e_1 - e_3}}{K(\kappa_r)} \tag{6.5}$$

and

$$\Upsilon_\theta = \frac{2\pi}{\Lambda_\theta} = \frac{\pi \sqrt{\bar{e}_1 - \bar{e}_3}}{K(\kappa_\theta)} \tag{6.6}$$

for the radial and $\theta$-motion respectively.
Furthermore, one can obtain the angular frequencies $\Upsilon_\varphi$ and $\Upsilon_t$ for the $\varphi$-motion and $t$-motion respectively from the solutions of $\varphi(\lambda)$ and $t(\lambda)$. By using the arguments outlined in [35], one notices that the solutions $\varphi(\lambda)$ and $t(\lambda)$ can be both expressed in the following forms

$$\varphi(\lambda) = \Upsilon_\varphi (\lambda - \lambda_0) + \varphi^{(r)}(\lambda) + \varphi^{(\theta)}(\lambda) \tag{6.7}$$

and

$$t(\lambda) = \Upsilon_t (\lambda - \lambda_0) + r^{(r)}(\lambda) + t^{(\theta)}(\lambda), \tag{6.8}$$

where $\Upsilon_\varphi$ and $\Upsilon_t$ correspond to frequencies in Mino time for $\varphi$-motion and $t$-motion respectively. From the solutions, one can obtain

$$\begin{aligned} \Upsilon_\varphi \;=\; & \frac{(\bar{L} + 2\ell \bar{E} x_\theta)}{(1 - x_\theta^2)} - a\bar{E} + \frac{a(r_1^2 - \bar{q} Q r_1 + a^2 + \ell^2 - a\bar{L})}{\Delta} \\ & + \sum_{i=1}^{2} \sum_{j=1}^{2} \left( \zeta(a_{ij}) \frac{(\bar{L}\bar{G}_i + 2\ell \bar{E} G_i)}{\wp'(a_{ij})} + \zeta(v_{ij}) \frac{a(\tilde{\omega}_i - \bar{q} Q \hat{\omega}_i + (a^2 + \ell^2 - a\bar{L})\breve{\omega}_i)}{\wp'(v_{ij})} \right) \end{aligned} \tag{6.9}$$

and

$$\Upsilon_t = \Upsilon_t^{(r)} + \Upsilon_t^{(\theta)}, \tag{6.10}$$

where

$$\begin{aligned}
\Upsilon_t^{(r)} &= \left[\bar{E}(r_1^2+\ell^2+a^2)^2 - \bar{q}Q(r_1^2+\ell^2+a^2)r_1 - a\bar{L}(r_1^2+1)\right]\frac{1}{\Delta(r_1)} \\
&+ \sum_{i=1}^{3}\sum_{j=1}^{2}\frac{(\bar{E}\omega_i - \bar{q}Q\bar{\omega}_i)}{\wp'(v_{ij})}\zeta(v_{ij}) - \frac{\bar{E}\beta_3^2}{16}\sum_{j=1}^{2}\frac{1}{\wp'^2(v_{3j})}\left(\wp(v_{3j}) + \frac{\wp''(v_{3j})}{\wp'(v_{3j})}\right) \\
&+ \sum_{i=1}^{2}\sum_{j=1}^{2}\left[\left(2\bar{E}(\ell^2+a^2) - a\bar{L}\right)\tilde{\omega}_i\right. \\
&\left. -\bar{q}Q(\ell^2+a^2)\hat{\omega}_i + (\ell^2+a^2)\left(\bar{E}(\ell^2+a^2) - a\bar{L}\right)\breve{\omega}_i\right]\frac{\zeta(v_{ij})}{\wp'(v_{ij})}
\end{aligned} \tag{6.11}$$

and

$$\begin{aligned}
\Upsilon_t^{(\theta)} &= a\bar{L} + a^2\bar{E}^2(x_\theta^2-1) + 4a\ell\bar{E}x_\theta - \frac{2x_\theta\ell}{1-x_\theta^2}\left(2\ell\bar{E}x_\theta + \bar{L}\right) \\
&-2\ell\sum_{i=1}^{2}\sum_{j=1}^{2}\frac{(\bar{L}G_i + 2\ell\bar{E}\bar{G}_i)}{\wp'(a_{ij})}\zeta(a_{ij}) \\
&+a\bar{E}\left(\frac{ax_\theta}{2} + \ell\alpha_3\right)\sum_{i=1}^{2}\frac{1}{\wp'(b_{1i})}\zeta(b_{1i}) \\
&-\frac{a^2\bar{E}\alpha_3^2}{16}\sum_{i=1}^{2}\frac{1}{\wp'^2(b_{1i})}\left(\wp(b_{1i}) + \frac{\wp''(b_{1i})}{\wp'(b_{1i})}\right).
\end{aligned} \tag{6.12}$$

Finally, as illustrated in [35], the angular frequencies calculated using Mino time $\lambda$ can be related to the angular frequencies $\Omega_r$, $\Omega_\theta$ and $\Omega_\varphi$ calculated with respect to a distant observer time as

$$\Omega_r = \frac{\Upsilon_r}{\Upsilon_t}, \qquad \Omega_\theta = \frac{\Upsilon_\theta}{\Upsilon_t}, \qquad \Omega_\varphi = \frac{\Upsilon_\varphi}{\Upsilon_t}. \tag{6.13}$$

Considering that these frequencies are not equal, it enables us to evaluate the precession of the orbital ellipse and Lense-Thirring effect for angular motions $\varphi$ and $\theta$. These can be given by

$$\Omega_{perihelion} = \Omega_\varphi - \Omega_r, \qquad \Omega_{LT} = \Omega_\varphi - \Omega_\theta. \tag{6.14}$$

Although we couldn't provide a numerical value for perihelion precision and Lense-Thirring effect, we can deduce that the NUT parameter and the charge of the test particle definitely influence these observables.

# 7 Conclusion

In this work, we have examined the motion of a charged test particle in Kerr-Newman-Taub-NUT spacetime. We have analyzed the angular and radial parts of the orbital motion by discussing possible orbit types that may appear. In the analysis of the angular part, we can see that the NUT parameter has a significant effect for the existence of equatorial orbits such that unlike in the background of Kerr and Kerr-Newman spacetimes where equatorial orbits does exist for any spacetime parameter, one cannot obtain equatorial orbits in Kerr-Taub-NUT and Kerr-Newman-Taub-NUT spacetimes for arbitrary spacetime parameters, the energy and the angular momentum of the test particle. Meanwhile, equatorial orbits exist either for vanishing NUT parameter ($\ell = 0$) or if a specific relation is satisfied between the energy and the orbital angular momentum of the test particle for non-vanishing NUT parameter. We have also classified the orbit types according to the number of real roots of the radial polynomial as well as the value of the energy of the test particle (whether it is smaller, greater than unity or equal to unity). We can strictly mention that, the existence of the NUT parameter does influence the radial and the angular part of the motion by causing different types of orbits to appear as can be seen from three dimensional plots of orbits. As in [14], we have examined the conditions for a bound orbit outside the outer singularity (i.e for the region where $r > r_+$) as well. Furthermore, we have discussed spherical orbits by obtaining the energy and angular momentum of the test particle in such an orbit by also investigating the stability. We have observed that stable spherical orbits change their class from retrograde orbits (where $a > 0, \bar{L} < 0$) to direct ones (where $a > 0, \bar{L} > 0$) as the NUT parameter varies. Next, we have obtained the analytical solutions of the orbit equations in terms of Weierstrass $\wp$, $\sigma$, and $\zeta$ functions. We have also provided three dimensional plots of the orbits for fixed values of the spacetime parameters and the energy of the test particle. We have seen that a bound orbit can exist for all possible values of the energy of the test particle (i.e for $\bar{E} < 1$, $\bar{E} > 1$ and $\bar{E} = 1$) when the spacetime parameters are fixed. Moreover, we have also calculated the perihelion precision and Lense-

Thirring effect for a bound motion. It can be seen from the relations of the observables that the NUT parameter and the charge of the test particle do strictly affect the perihelion precision and Lense-Thirring phenomena.

For future work, it is also of interest to examine the planar orbits of the charged test particles in Kerr-Newman-Taub-NUT background. It would be remarkable to examine the orbits over a fixed $\theta = \theta_0$ plane for arbitrary values of the angular momentum and the energy of the test particle and the spacetime parameters. One can also study the equatorial orbits with the relation (4.9) imposed. Furthermore, one can similarly investigate the effect of the cosmological constant on the orbital motion of a test particle in a spacetime where both the NUT and rotation parameters exist [8]. These are devoted to future research.

# Acknowledgement

We would like to thank Mehmet Ergen for fruitful discussions and for his help for obtaining especially three dimensional plots of the orbits.

# References

[1] E. Newman, L. Tamburino, T. Unti, *Empty space generalization of the Schwarzschild metric*, J. Math. Phys. **4**, 915 (1963).

[2] M. Demiański and E. T. Newman, Bull. Acad. Polon. Sci., Ser. Sci., Math., Astron., Phys. **14**, 653 (1966).

[3] C. W. Misner, *The Flatter regions of Newman, Unti and Tamburino's generalized Schwarzschild space*, J. Math. Phys. **4**, 924 (1963).

[4] J. G. Miller, *Global analysis of the Kerr-Taub-NUT metric*, J. Math. Phys. **14**, 486 (1973).

[5] W. B. Bonnor, Proc. Cambridge Phil. Soc. **66**, 145 (1969).

[6] D. Bini, C. Cherubini, R. T. Jantzen, B. Mashhoon, *Gravitomagnetism in the Kerr-Newman-Taub-NUT spacetime*, Class. Quant. Grav. **20**, 457 (2003).

[7] D. Bini, C. Cherubini, R. T. Jantzen, *On the interaction of massless fields with a gravitomagnetic monopole*, Class. Quant. Grav. **19**, 5265 (2002).

[8] A. N. Aliev, *Rotating spacetimes with asymptotic non-flat structure and the gyromagnetic ratio* , Phys. Rev. D **77**, 044038 (2008).

[9] G. D. Esmer, *Separability and hidden symmetries of Kerr-Taub-NUT spacetime in Kaluza-Klein theory* , Grav.Cosmol. **19**, 139 (2013).

[10] C. Liu, S. Chen, C. Ding, J. Jing, *Particle Acceleration on the Background of the Kerr-Taub-NUT Spacetime* , Phys. Lett. B **701**, 285 (2011).

[11] D. Lynden-Bell, M. Nouri-Zonoz, *Classical monopoles: Newton, NUT space, gravimagnetic lensing and atomic spectra*, Rev. Mod. Phys. **70**, 427 (1998).

[12] G. G. L. Nashed, *Total conserved charges of Kerr-NUT spacetimes using Poincare version of teleparallel equivalent of general relativity*, Eur. Phys. J. C **72**, 2010, (2012).

[13] Y. Hagihara, Japan J. Astron. Geophy. **8**, 67, (1931).

[14] D. C. Wilkins, *Bound geodesics in the Kerr metric*, Phys. Rev. D **5**, (1972) 814.

[15] J. M .Bardeen, W. H. Press and S. A. Teukolsky, *Rotating black holes: Locally nonrotating frames, energy extraction and scalar synchrotron radiation*, The Astrophys. Journal **178**, 347 (1972).

[16] S. Chandrasekhar, *The Mathematical Theory of Black Holes* (London: Clarendon Press) (1983).

[17] B. O'Neill, *The Geometry of Kerr Black Holes* (Massachusetts: A K Peters/CRC Press) (1995).

[18] R. Fujita, W. Hikida, *Analytical Solutions of bound timelike geodesic orbits in Kerr spacetime*, Class. Quant. Grav. **26**, 135002 (2009).

[19] E. Hackmann, C. Lämmerzahl, *Geodesic equation in Schwarzschild-(anti-) de Sitter space-times: Analytical solutions and applications*, Phys. Rev. D **78**, 024035 (2008).

[20] E. Hackmann, C. Lämmerzahl, *Complete Analytic Solution of the Geodesic Equation in Schwarzschild-(anti-) de Sitter Spacetimes*, Phys. Rev. Lett. **100**, 171101 (2008).

[21] E. Hackmann, C. Lämmerzahl, *Analytical solution of the geodesic equation in Kerr-(anti-) de Sitter space-times*, Phys. Rev. D **81**, 044020 (2010).

[22] E. Hackmann, B. Hartmann, C. Lämmerzahl, P. Sirimachan, *Test particle motion in the spacetime of a Kerr black hole pierced by a cosmic string*, Phys. Rev. D **82**, 044024 (2010).

[23] K. Flathmann, S. Grunau, *Analytic solutions of the geodesic equation for Einstein-Maxwell-dilaton-axion black holes*, Phys. Rev. D **92**, 104027 (2015).

[24] E. Hackmann, V. Kagramanova, J. Kunz, C. Lämmerzahl, *Analytic solutions of the geodesic equation in higher dimensional static spherically symmetric spacetimes*, Phys. Rev. D **78**, 124018 (2008).

[25] S. Grunau, V. Kagramanova, J. Kunz, C. Lämmerzahl, *Geodesic motion in the singly spinning black ring spacetime*, Phys. Rev. D **86**, 104002 (2012).

[26] S. Grunau, V. Kagramanova, J. Kunz, *Geodesic motion in the (charged) doubly spinning black ring spacetime*, Phys. Rev. D **87**, 044054 (2013).

[27] S. Grunau, V. Kagramanova, *Geodesics of electrically and magnetically charged test particles in the Reissner-Nordström spacetime: Analytical solutions* , Phys. Rev. D **83**, 044009 (2011).

[28] E. Hackmann, H. Xu, C. Lämmerzahl, *Charged particle motion in Kerr-Newmann space-times*, Phys. Rev. D **87**, 124030 (2013).

[29] Y. Mino, *Perturbative approach to an orbital evolution around a supermassive black hole*, Phys. Rev. D **67**, 084027 (2003).

[30] B. Carter, *Hamilton-Jacobi and Schrodinger separable solutions of Einstein's equations* ,Commun. Math. Phys. **10**, 280 (1968); B. Carter, Phys. Rev.,*Global structure of the Kerr family of gravitational fields*, **174**, 1559 (1968).

[31] V. P. Frolov and D. Kubizňák, *Higher-dimensional black holes: Hidden symmetries and separation of variables* ,Class. Quantum Grav. **25**, 154005 (2008); V. P. Frolov, P. Krtous, and D. Kubizňák, *Separability of Hamilton-Jacobi and Klein-Gordon equations in general Kerr-NUT-AdS spacetimes*, J. High Energy Phys. **02**, 005 (2007).

[32] A. N. Aliev, G. D. Esmer, *Hidden symmetries and geodesics of Kerr spacetime in Kaluza-Klein theory* , Phys. Rev. D **87**, 084022 (2013).

[33] R. J. Howes, *Existence and stability of circular orbits in a Schwarzschild field with nonvanishing cosmological constant*, Aust. J. Phys. **32**, 293 (1979).

[34] Z. X. Wang, D. R. Guo, *Special Functions*, World Scientific, (1989).

[35] S. Drasco, S. A. Hughes, *Rotating black hole orbit functionals in the frequency domain*, Phys. Rev. D **69**, 044015 (2004).